Novel Polymeric Dielectric Materials for the Additive Manufacturing of Microwave Devices

Shamus E O'Keefe

A dissertation
submitted in partial fulfillment of the
requirements for the degree of

Doctor of Philosophy

University of Washington
2017

Reading Committee:
Christine Luscombe, Chair
Marjorie Olmstead
Guozhong Cao

Program Authorized to Offer Degree:
Materials Science and Engineering

University of Washington

Abstract

Novel Polymeric Dielectric Materials for the Additive Manufacturing of Microwave Devices

Shamus E O'Keefe

Chair of the Supervisory Committee:
Professor Christine K. Luscombe
Materials Science and Engineering

The past decade has seen a rapid increase in the deployment of additive manufacturing (AM) due to the perceived benefits of lower cost, higher quality, and a smaller environmental footprint. And while the hardware behind most of AM processes is mature, the study and development of material feedstock(s) are in their infancy, particularly so for niche areas. In this dissertation, we look at novel polymeric materials to support AM for microwave devices. Chapter 1 provides an overview of the benefits of AM, followed by the specific motivation for this work, and finally a scope defining the core objectives. Chapter 2 delves into a higher-level background of dielectric theory and includes a brief overview of the two common dielectric spectroscopy techniques used

in this work. The remaining chapters, summarized below, describe experiments in which novel polymeric materials were developed and their microwave dielectric properties measured.

Chapter 3 describes the successful synthesis of polytetrafluroethylene (PTFE)/polyacrylate (PA) core-shell nanoparticles and their measured microwave dielectric properties. PTFE/PA core-shell nanoparticles with spherical morphology were successfully made by aersol deposition followed by a brief annealing. The annealing temperature is closely controlled to exceed the glass transition (T_g) of the PA shell yet not exceed the T_g of the PTFE core. Furthermore, the annealing promotes coalescence amongst the PA shells of neighboring nanoparticles and results in the formation of a contiguous PA matrix that has excellent dispersion of PTFE cores. The measured dielectric properties agree well with theoretical predictions and suggest the potential of this material as a feedstock for AM microwave devices.

Chapter 4 delves into the exploration of various polyimide systems with the aim of replacing the PA in the previously studied PTFE/PA core-shell nanoparticles. Fundamental relationships between polymer attributes (flexibility/rigidity and functional groups) and dielectric properties were explored. The results indicate that backbone rigidity and the inclusion of fluorine lead to excellent dielectric properties, however, often at the expense of mechanical properties.

Chapter 5 explores the optimization of PTFE core-shell nanoparticles via a novel PTFE/polyimide (PI) core-shell nanoparticle. PTFE/PI core-shell nanoparticles were synthesized via electrostatic interaction between the PTFE cores and a PI precursor, poly(amic) acid salt (PAAS). The PAAS is converted to PI by thermal imidization. The PI has properties superior to those of PA for microwave applications and the results suggest the promise of PTFE/PI core-shell nanoparticles for use in AM of microwave devices.

Chapter 6 describes the first report of on actively-tunable microwave substrate made possible by a semiconducting polymer composite blend. The composite blend is comprised of poly(3-hexylthiophene) (P3HT) as the semiconducting polymer and [6,6]-Phenyl C61 butyric acid methyl ester (PCBM) while the remainder of the composite is comprised of a low dielectric constant polymer polydimethylsiloxane (PDMS). When subjected to photo excitation (white light, spectrum centered at 532 nm), the composite exhibits a tunability of the permittivity up to 20%. The results suggest strong promise for the use of semiconducting polymers in actively-tunable microwave devices.

Finally, Chapter 7 presents a summary of the salient conclusions of the reported studies. The chapter concludes with a few brief remarks of my personal experience as a non-traditional student and the challenges therein.

ACKNOWLEDGEMENTS

First and foremost I would like to thank my advisor, Dr. Christine Luscombe. Thank you for the patience you have shown the past three years. Perhaps the biggest compliment I can offer is that I learned as much science and engineering as I did about myself.

I'd also like to thank the other members of my Supervisory Committee for their support, advisement, and encouragement.

I'd like to thank Raytheon Company for granting me this opportunity through the Advanced Study Program. Specifically, thank you to Dr. Chris McCarroll and Dr. Mary Herndon for their encouragement and support.

Finally, thank you to my wife and family for the love and support that made this possible.

DEDICATION

To my mom, for everything

Table of Contents

List of Figures

List of Tables

ACRONYMS

AFM: atomic force microscope

AM: additive manufacturing

BA: butyl acrylate

DI: deionized

DLS: direct laser sintering

EMT: effective medium theory

FTIR: Fourier transform infared

MMA: methyl methacrylate

P3HT: poly(3-hexylthiophene)

PA: polyacrylate

PAAS: poly(amic) acid salt

PCBM: [6,6]-Phenyl C61 butyric acid methyl ester

PDMS: polydiemthylsiloxane

PI: polyimide

PMMA: polymethylmethacrylate

PTFE: polytetrafluoroethylene

SEM: scanning electron microscopy

TEM: transmission electron microscopy

TRL: thru-reflect line

VNA: vector network analyzer

1. Introduction

Additive Manufacturing (AM) is defining the current era of electronics manufacturing. Specifically, AM offers benefits that other manufacturing technologies cannot compete with. The advantages of AM include, but are not limited to, lower overall costs, improved device performance, reduced environmental footprint, and several other indirect downstream & upstream benefits. Table 1 contains a feature-benefit analysis of AM.

Table 1. Feature-benefit analysis of AM.

Feature	Benefit
Fewer Process Steps	Lower Operational Costs
Additive vs. Subtractive Process	Reduced Material Waste
Superior Properties	Improved Performance
Novel Shapes/Sizes	Design Freedom & Parallel Customization
Digital Data Driven	Lower Initial Cost, Faster to Market

Production costs are always pressured for reductions and AM is a means towards that end. Take for example conformal antennas found in many cellular devices where special plating processes and tooling setups are required under traditional manufacturing schemes. Certainly AM could eliminate several of these steps. And as a result, significant cost reduction, together with fewer safety exposures, can be achieved. Savings can also be realized in upstream design activities. When design changes are implemented, tooling changes are often required, increasing cost and adding time to the change cycle. In addition to reducing costs, AM also can reduce the impact to raw materials and waste streams. General Electric is one of the forerunners ushering in AM and are now producing a superalloy engine nozzle using a Direct Laser Sintering (DLS) process. Previous manufacturing methods required 50% more raw material and produced waste streams with little to no capacity for recycling. In sum total, AM schemes have demonstrated remarkable advantages,

including reduced cost, higher quality products, improved performance, and reduced environmental impact.

1.1. Motivation

Remarkably, the vast majority of the equipment and hardware used in nearly all additive processes is based or borrowed from widely available, mature technology that is ubiquitous in today's factories, e.g. computer numerically controlled (CNC) controls. Despite this, the evolution of AM from a material perspective has just begun. Indeed, a significant opportunity to advance the field of AM lies in the development of new materials. Nearly all AM schemes process raw materials in ways that often require unique properties compared to typical processing routes. For example, a DLS produced rocket nozzle requires superalloy nanoparticles with tightly controlled tolerances, such as narrow size distribution, high degree of dispersion, geometric criteria, and several others. Another example is raydome electro-magnetic interference (EMI) shields directly ink-deposited that require ink with properties unique to that process such as viscosity, solvent content, and solids loading. While much work has been pioneered in the area of materials for AM, there remains dozens if not hundreds of cases where a lack of material development has prevented the adoption of an AM process. A perfect example of such a case is the manufacturing of microwave devices, specifically substrates.

Microwave substrates are often required to possess unique electrical properties, namely low permittivity, i.e. dielectric constant, to maintain signal integrity. Polytetrafluoroethylene (PTFE) has the lowest permittivity of any known solid material (excluding aerogels) and as a result, has long been a favored material for microwave substrates, yet the manufacturing remains a batch

process where individual pieces are reduced from bulk stock. Hence, PTFE perfectly illustrates how a material's properties have impeded the adoption of AM, in this case for microwave substrates. As an example, PTFE's extremely high melt viscosity prohibit any possibility of a melt extrusion. Furthermore, PTFE is insoluble in all common solvents, rendering it extremely difficult to process in a solution based environment. In addition to PTFE, there are likely dozens of technologically critical materials that have yet to be tailored suitable for AM use. If one compares literature statistics (correlated to industry), the state of technology is apparent. **Table 2** shows hits for literature searches in the Web of Science database. Published data on dielectric inks used in AM for high frequency use is virtually non-existent.

Table 2. Results of literature search in Web of Science April 2017.

Topic	**Result (hits)**
"Conductive Ink"	136
"Cu ink"	35
"Dielectric ink"	17
"Dielectric ink" + "microwave"	0
"Dielectric ink" + "radio frequency (RF)"	0

As one might expect, it is no surprise that there are zero commercial offerings for dielectric materials, in an ink or paste form, capable of meeting the requirements typical of X band use. Table 3 shows typical performance requirements for dielectric materials that operate in the X band frequencies. Companies that produce X band microwave devices are at ground zero for dielectric inks capable of meeting the performance requirements. Without a concerted research effort, materials like PTFE and numerous others will remain unsuitable for most AM processes.

Table 3. Desired properties of dielectric materials in the X band (7-12 GHz).

Desired Property	Value
Stable dielectric constant, ε’	~2.0-4.0 (passive devices)
Low insertion loss, ε’’	.0001-.0003
Thermal conductivity (W/m/K)	1.5
Coefficient of thermal expansion (ppm/°C)	19 (x & y) 39 (z)

In addition to basic substrates, there exists other high performance microwave devices that enable enhanced electrical performance. For instance, actively tunable materials can modulate electrical properties, including permittivity and permeability, in real-time. Such capability gives rise to a host of useful devices including phase shifters, variable integrated capacitors, filters, and voltage-controlled oscillators. Understandably, these microwave photonic devices have seen significant research efforts in the last decade driven by a need for dynamic control and ultrafast response times. Given the ease of processing inherent in many polymer systems, it is no wonder that P3HT, a semiconducting polymer, has emerged as the prototypical material for AM of electronic devices. P3HT owes its popularity to its relatively high charge mobility and optical absorption properties. Additionally, its small band gap makes it particularly attractive. Given a 1.9 eV band gap and absorption peaks between 450 and 600 nm, it is ideally suited for the photogeneration of charges using visible light. Thus, it is possible to conceive a P3HT based composite substrate that by virtue of optical excitation, could actively tune the dielectric properties.

1.2. Scope

Polymers make up the vast majority of materials used in AM. Polymers have been the prominent material in AM for several decades. Of the leading commercial AM machine vendors, from 1988-2011, all have the capability to utilize polymers as feedstock raw material. Utilizing polymers in

AM can offer many advantages from a performance, processing, and cost standpoint. These advantages can include high strength/weight ratios, manufacturing flexibility, tailorable properties, and dimensional stability.[1] In addition, the AM processes that use polymers are varied including material extrusion, aerosol jetting/spraying, vat polymerization, powder bed fusion, and binder jetting.[2] It is evident that an opportunity exists, both academically and commercially, to design and develop polymer based dielectric materials for AM of microwave devices.

The scope of this dissertation is to develop and characterize novel polymeric materials suitable for AM of microwave devices. For basic substrate materials, PTFE is the preferred material and was purchased as a dispersion of ~200 nm particles and used as received. This dispersion was used as seed particles for core-shell particles with PTFE being the core and in one case, polyacrylate (PA) being the shell and in another case, poly(amic) acid salt (PAAS) being the shell. Both PA and PAAS are synthesized via facile, low temperature routes performed under a chemical hood with standard laboratory equipment. Similar to PAAS, the polyimides studied were synthesized *via* similar routes. Finally, the P3HT composites used to study actively tunable materials were synthesized via simple blending techniques followed by ordinary mold casting; the P3HT was purchased and used as received.

In addition to the materials, a significant portion of the scope included the study and subsequent fabrication of a test bed to measure dielectric properties. There are several different techniques used to measure dielectric properties. However, when measuring dielectric properties in the microwave range (1-30 GHz), cavity perturbation is often preferred due to the accuracy and simplicity of the operation. One simply needs a Vector Network Analyzer (VNA) and a suitable cavity, which is often a section of waveguide of the operating frequency to be measured. In

addition to the VNA and cavity, ancillary equipment including simple fixtures for sample loading were designed and fabricated.

2. Background

2.1. Dielectric theory of polymers

2.1.1. Polarization

The Clausius-Mossotti equation describes a dielectric under the influence of an applied field.[3] It relates a microscopic property, polarizability, to a macroscopic property, dielectric constant ε_r:

$$\frac{\varepsilon_r - 1}{\varepsilon_r + 2} \cdot \frac{M}{\rho} = \frac{N_A \alpha}{3\varepsilon_0} \quad (1)$$

Where α is the polarizability, ε_r is the relative permittivity, ε_0 is the permittivity of a vacuum, M is the molecular weight, N_A is Avogadro's constant, and ρ is density. Simple manipulation shows that the dielectric properties are dependent on polarizability and free volume. Polarizability is unique to each type of atom or molecule and is the proportionality constant for the formation of dipole(s) under an applied electric field. Physically, polarizability exists only under influence of an applied field. There are several different polarizing mechanisms, each with a unique manner in which the material reacts with the applied field.[4] Each can be considered a resonance or relaxation type. In addition, each mechanism is prevalent at a characteristic frequency, also the reciprocal of the relaxation time of the mechanism.

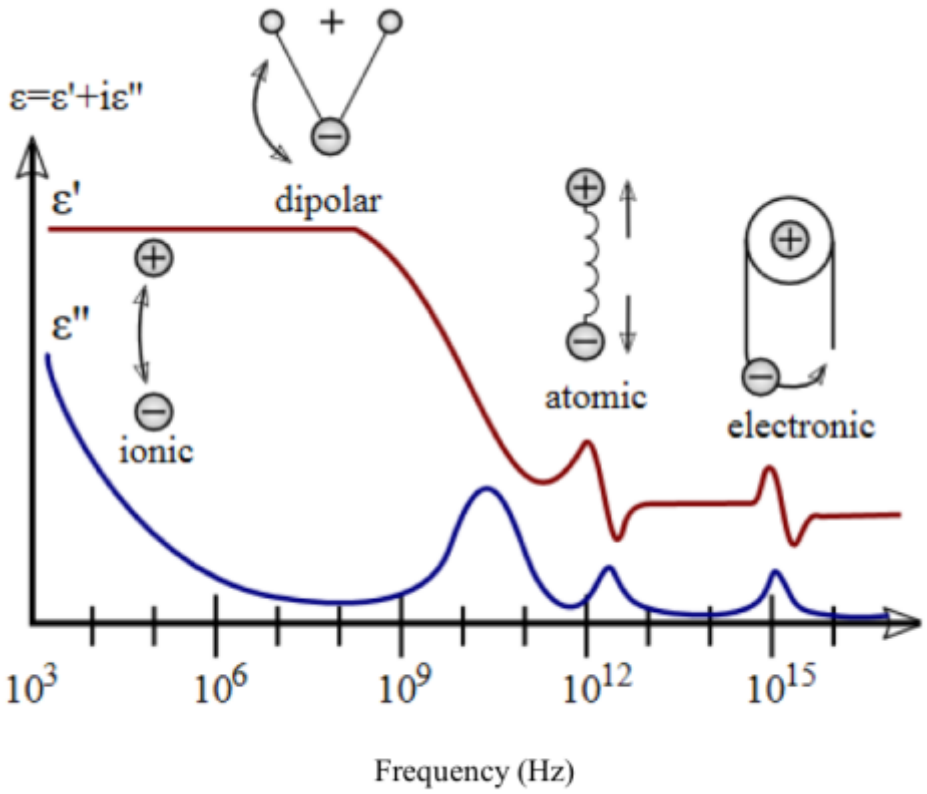

Figure 1. Dielectric permittivity spectrum over a wide range of frequencies.

Figure 1 depicts the various polarization mechanisms vs. log frequency.[5] The different mechanisms include:

- **Electronic polarization:** With no applied field, electrons are in their equilibrium positions around the nucleus in a more or less even distribution. When the field is applied, the electron cloud is displaced from this equilibrium position, the extent of which depends on many factors. If the electron cloud is displaced away from a positive nucleus, a dipole is formed. It is considered a resonant mechanism.
- **Atomic polarization:** A resonant process that is a vibrational excitation, occurring when there is a non-zero dipole moment to the vibrational mode.

- **Dipole polarization:** A relaxation process that occurs when permanent or induced dipoles align with an applied field.
- **Ionic polarization:** A relaxation process that occurs when a sub lattice is displaced from its equilibrium position in the lattice as a result of thermal motion, and as such is highly temperature dependent. The ions exhibit a dipole moment.

Under the influence of a static applied field (DC), static dipoles are created giving a dielectric constant of ε_{static}. However, under an applied alternating field (AC), the polarization will oscillate with the AC field. In this condition, all modes of polarization may contribute to the permittivity and each mode is dependent on the frequency of the applied field. If one takes the reciprocal of the frequency in Figure 1, the time scale of each mechanism is evident. Electronic polarization is nearly instantaneous, as electrons have relatively low mass and therefore able to follow the alternating field in phase. Elements/molecules with prevailing mechanisms on the left of Figure 1 can be highly polarizable whereas those on the right can be relatively low, but this behavior can change with frequency and be the inverse relationship; lower polarizability yields lower dielectric constant and vice versa. Take bromine, a highly polarizable element, and fluorine with low polarizability as examples. Bromine is the larger of the two elements and with a larger electron cloud, the coulombic force of the nucleus diminishes due in part to the large separation between the large cloud and nucleus and the presence of other electrons that shield the nucleus. Therefore, bromine's intrinsic electrical field (think electron cloud) is quite malleable; it doesn't take much of an applied field to distort the cloud. Fluorine, on the other hand, is the most electronegative of the elements and it holds its electrons very tightly, thus the electron cloud is not easily deformed. Another illustration is π bond *vs.* σ bond. The weaker π bond makes distortion of the electron cloud easier, resulting in high polarizability.

When examining polymers for dielectric applications at microwave frequencies, the predominant mechanism is dipolar relaxation, given that the speed of this mechanism falls in the first decade of the microwave range. However, at least one recent report claims that in the case of symmetrically substituted trifluoromethyl groups, both dipolar and electronic polarizablility have contributions, while atomic contributions are negligible.[6] Because incorporated ions would introduce a charge carrying capacity, it reasons that dielectric polymers rarely, if ever, contain ion species. For this reason, ionic polarization is not considered relevant for this work. It follows then, that the critical polarization mechanisms for dielectric applications in the microwave frequencies are dipolar and electronic.

In addition to polarizability, the free volume plays an equally significant role in the dielectric constant.[7] Free volume is simply the unoccupied space, primarily a result of end units being less dense than inter-chain units. Figure 2 illustrates polymer free-volume.

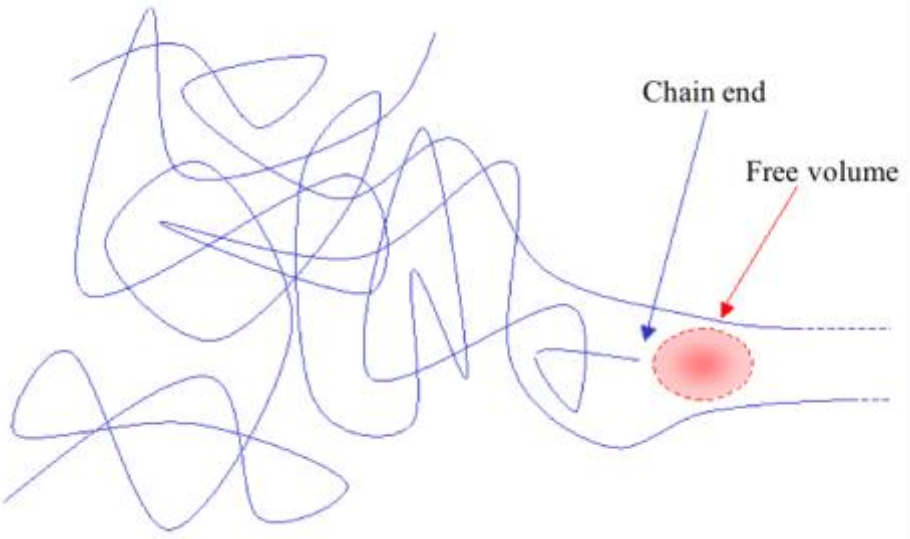

Figure 2. Polymer free volume as a result of chain end(s).

Obviously, the longer the chains present, the fewer chain ends, and thus less free volume. Since free volume has a dielectric constant of 1, a material with greater free volume will have a lower dielectric constant. In addition to chain length, backbone rigidity contributes significantly to free volume. Rigid, linear polymers promote efficient chain packing, leading to the absence of or minimized free volume. This results in increasing the dielectric constant. On the contrary, flexible, less rigid polymers have the ability to fold onto themselves, often entangled in one another. Such entanglements promote an increase in free volume, which as stated previously, decreases the dielectric constant.

The free volume may be estimated by the volume difference between repeat unit molar volume and total molar volume.[8] Macroscopic free volume in the form of porosity also greatly affects the dielectric constant. The reason for this is because the free volume is comprised mostly of air, which has a dielectric constant of 1, therefore decreasing the bulk volume dielectric constant. Various strategies to manipulate the dielectric constant center on adjusting/designing free volume, both macroscopically and at the molecular level.

2.1.2. Dielectric loss

Relative permittivity is expressed as:

$$\varepsilon_r = \varepsilon' - j\varepsilon'' \quad (2)$$

where ε', dielectric constant, is the real part and ε'', dielectric loss, is the imaginary part. The magnitudes of ε' and ε'' depend on the frequency of the applied field and are related by the Kramers-Kronig relation:[9]

$$\varepsilon'(\omega) = \varepsilon_0 + \frac{2}{\pi}\int_0^{\infty} \frac{u\varepsilon''(u)}{u^2 - \omega^2} du \quad (3)$$

The real part of the permittivity is given by:

$$\varepsilon' = \varepsilon_0 \varepsilon_r \quad (4)$$

The loss tangent is defined as the ratio between dielectric loss and the dielectric constant:

$$\tan\delta = \frac{\varepsilon''}{\varepsilon'} \quad (5)$$

Dielectric loss is best explained as the dissipation of energy, usually in the form of heat, when the polarization mechanism(s) are unable to keep pace with the alternating AC field. A material has a unique relaxation time that describes the time required for dipoles to return to their equilibrium orientations. While it's true that electronic polarization is nearly instantaneous, generally speaking relaxation is not instantaneous; the polarization decays exponentially after a disturbance from an external field. When the relaxation time is larger than the frequency of the field (oscillating time of the field), there will be loss.

2.1.3. Relaxation

The earliest and most simple model for relaxation is the Debye model,[10] best presented graphically in Figure 3.

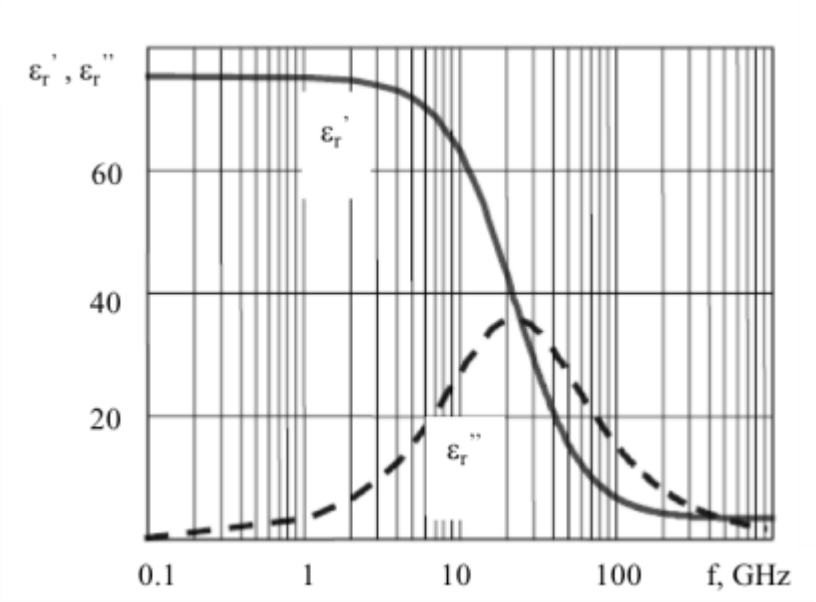

Figure 3. Debye dispersion curve.

In equation form:

$$\varepsilon' = \varepsilon_\infty + \frac{\varepsilon_s - \varepsilon_\infty}{1 + \omega^2\tau^2} \tag{6}$$

$$\varepsilon'' = \frac{\varepsilon_s - \varepsilon_\infty}{1 + \omega^2\tau^2}\omega\tau \tag{7}$$

Where ε_s is the static, low frequency permittivity, ε_∞ is the high frequency permittivity, τ is the relaxation time, ω and is the frequency. The Debye model relates a microscopic property, relaxation time τ, to the macroscopic dielectric properties ε' and ε''. Minor manipulation and eliminating $\omega\tau$ yields the relationship between ε' and ε'':

$$\left(\varepsilon' - \frac{\varepsilon_s + \varepsilon_\infty}{2}\right)^2 + \varepsilon''^2 = \left(\frac{\varepsilon_s - \varepsilon_\infty}{2}\right)^2 \tag{8}$$

2.2. Dielectric spectroscopy

Numerous techniques exist for the measurement of microwave dielectric properties. Each technique has unique advantages and disadvantages, and the correct technique for a particular application is largely dependent on the unique restrictions of each technique. Typically, the sample size and shape play a significant role, as does the desired accuracy and resolution of the measurement. However, the complexity of the equipment, ease of the measurement procedure, and the desired frequency range are also important decision criteria when choosing a measurement technique.

There are two fundamental types of measurement techniques for microwave property measurements: transmission/reflection techniques and resonance techniques. Transmission/ reflection techniques have the ability to sweep a wide frequency range, which is its primary advantage, whereas resonance techniques, while capable of only very narrow frequency ranges, have extremely high accuracy. Both techniques are widely used and are proven methods to obtain valid microwave dielectric properties.

The transmission/reflection technique involves measuring the complex scattering parameters S_{11} (reflection) and S_{21} (transmission), i.e. S-parameters, of a sample placed into a section of waveguide or coaxial line or can be a two-port microstrip fixture. A computationally intense conversion method extracts the complex dielectric properties from the measured S-parameters, most often carried out using specialized computational software. Again, a wide range of frequencies can be measured using this technique, and as such, has the capability to elucidate the onset of relaxation mechanisms in the material. The non-iterative conversion method used in this work can be seen in section 6.2.

Resonance techniques are widely used for measuring microwave dielectric properties, of which there are two main types: 1) The material is machined or formed to a desired shape and acts as a dielectric resonator, and 2) A sample of material is inserted into a resonator, which causes a small perturbation of the field distributions within the cavity, hence the name, cavity perturbation. In this study, the cavity perturbation technique was chosen due to the simplicity of the procedure, the relatively small sample size, and the basic mathematical extraction of dielectric properties. It is worth noting that for the studies involving actively tunable materials, a transmission/reflection technique was used employing a two-port microstrip test fixture.

3. Polytetrafluoroethylene-Polyacrylate Composite Films

*The majority of this section has been previously published.[11]

3.1. Introduction

The objective of this research is to assess the candidacy of polymers for their use as a material for the AM of microwave devices. This can be achieved through a comprehensive investigation of the structure-property relationship. The main focus is to study and understand the dependence of the dielectric properties on the physical and chemical characteristics of the polymers; however, thermal, mechanical, rheological, and other properties will be elucidated as well. To date, there is little published data on the microwave X band (7-12 GHz) dielectric properties of polymers. Once a knowledge of the structure-property relationship is established, it can then be the basis for further optimization. Table 4 shows the dielectric properties of various polymers and water.[12]

Table 4. Dielectric properties of various polymers (1 GHz).

Polymer	Dielectric Constant, ε'	Dielectric Loss, ε''
Polystyrene (PS)	2.5-2.6	.00033
Polyethylene (PE)	2.26	.00031
Polytetrafluoroethylene (PTFE)	2.1	.00028
Water	80	.157

PTFE is widely used as a microwave substrate due to its low and stable dielectric constant ε' (2.1) and extremely small dielectric loss ε'' (.00028).[13] Particularly with regard to microwave devices, these properties enable device performances that would otherwise be unattainable. Specifically, the low dielectric constant permits a high signal transmission, while the low dielectric loss helps minimize the power required to drive the signal.[14] These outstanding dielectric properties are primarily a result of the low polarizability of the PTFE molecule. While the very strong C-F bond is highly polar, the spatial arrangement of repeat units along the carbon backbone results in a near-

zero vector sum, yielding a zero dipole moment.[15] Yet, despite the attractive properties of PTFE, it is difficult to process it using standard thermoplastic processing techniques. Because of its high molecular weight and internal resistance to rotation within repeating units, PTFE has difficulty crystallizing from the melt. Furthermore, it is typically necessary to sinter PTFE versus extruding or molding via common processing techniques.[16] Combined, these characteristics present a challenge for using non-contact deposition techniques to create a dense, physically and chemically homogenous solid.[17]

To produce a dense solid from dry PTFE particles, they must be sintered at a temperature above its melting point of 325 °C.[18] While this technique is widely used in PTFE coatings, the elevated temperature would be deleterious to many materials already present in an electronic device. For instance, temperatures above 200 °C in Si devices can cause high leakage currents and eventually lead to total device failure.[19] Other damaging effects include thermal stresses, accelerated/enhanced diffusion, and recrystallization, to name a few. In order to deposit PTFE in a high-throughput fashion while maintaining device/material integrity, lower temperature techniques must be developed. An alternative method is to print an aqueous dispersion of PTFE particles; however, this technique (printing with no post heat treatment) leads to a low density film comprised of unsintered PTFE particles.[20] The volume of void space present in such a film is undesirable as it affords the opportunity for the uptake of water. Because water has a dielectric constant of 80, its presence significantly increases the dielectric constant of the film to values not suitable for the intended use.

In the first stage of this work, we developed an alternative low-temperature process for printing dense substrates from PTFE nanoparticles. This method homogenously incorporates PTFE nanoparticles within a secondary polymer matrix of PA by using a core-shell PTFE nanoparticle

architecture. Specifically, if the glass transition temperature of the shell polymer ($T_{g,s}$) is tailored to be lower than the glass transition temperature of the PTFE core ($T_{g,c}$), a brief annealing at an intermediate temperature ($T_{g,s}<T<T_{g,c}$) will allow the shell material to soften, thereby becoming a binder between adjacent PTFE particles. The end result will yield a composite with a dispersion of PTFE particles within an annealed shell polymer matrix, as depicted in Figure 4. It is noteworthy that a PA polymer matrix is not expected to yield dielectric properties suitable for commercial use (ε' = ~ 2.0 and ε'' = ~ 10^{-4}); however, the relatively low T_g of PA provides a model system to assess the aerosol deposition as a means of producing a dense film.

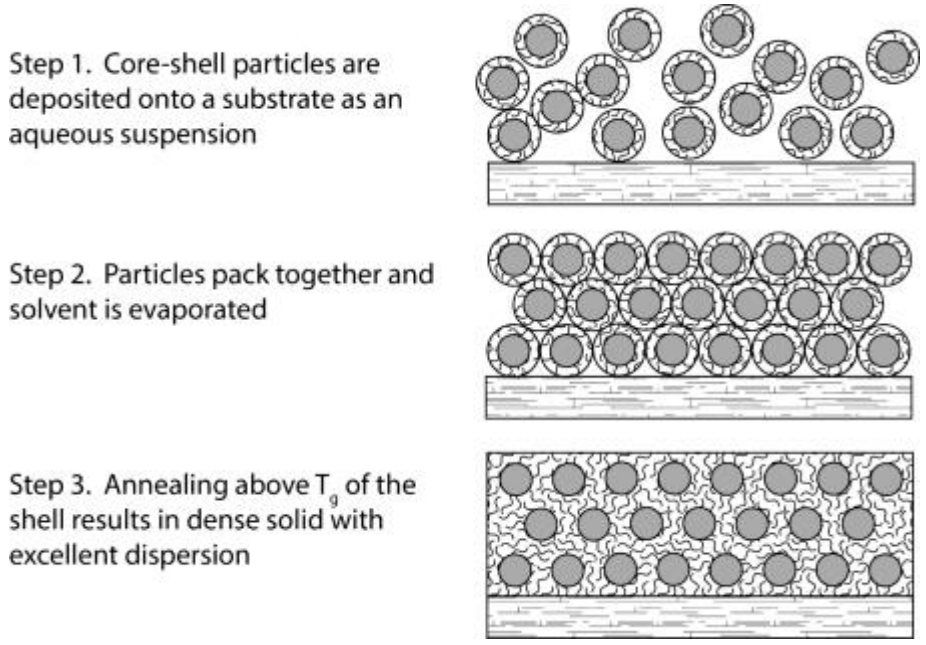

Figure 4. Representation of deposited core-shell particles becoming a dense solid.

This technique was implemented to produce composite films with dielectric properties comparable to several theoretical predictions. Dielectric properties of the PTFE-PA core-shell nanoparticles composites were examined with an increasing weight fraction of PTFE, up to a maximum of 50%. A simple aerosol deposition technique was employed to aerosol spray films onto bare soda-lime

glass substrates. Because permittivity is the critical property of microwave dielectric materials, these samples were examined with a highly sensitive dielectric spectroscopy technique. Specifically, a modified cavity perturbation resonance technique was employed to investigate the dielectric constant and dielectric loss of the films at a frequency of 7.2 GHz.[21] The results of this study will aid in determining the viability of utilizing PTFE-PA core-shell nanoparticles in AM processes, particularly those used for microwave dielectric production.

3.2. Experimental

Materials

Butyl acrylate (BA, 99+%, TCI America), methyl methacrylate (MMA, 99+%, TCI America), methacrylic acid (MA, 99%, TCI America) were used as received. Monomers were refrigerated at 5 °C until used. Potassium persulfate (KPS, Sigma-Aldrich) was used as received. The PTFE dispersion was obtained from Sigma-Aldrich and contained a 60% solids loading with a reported mean particle size of 200 nm. All water used was deionized.

Synthesis

The PTFE-PA core-shell nanoparticles were synthesized by a seeded emulsion polymerization using PTFE as the seed material and acrylate monomers for the shell. A simplified representation of seeded emulsion polymerization can be seen in Figure 5. All polymerizations were performed in a 250 mL three-neck flask with reflux condenser, magnetic stirrer, heated oil bath, all under a nitrogen atmosphere as described elsewhere.[22]

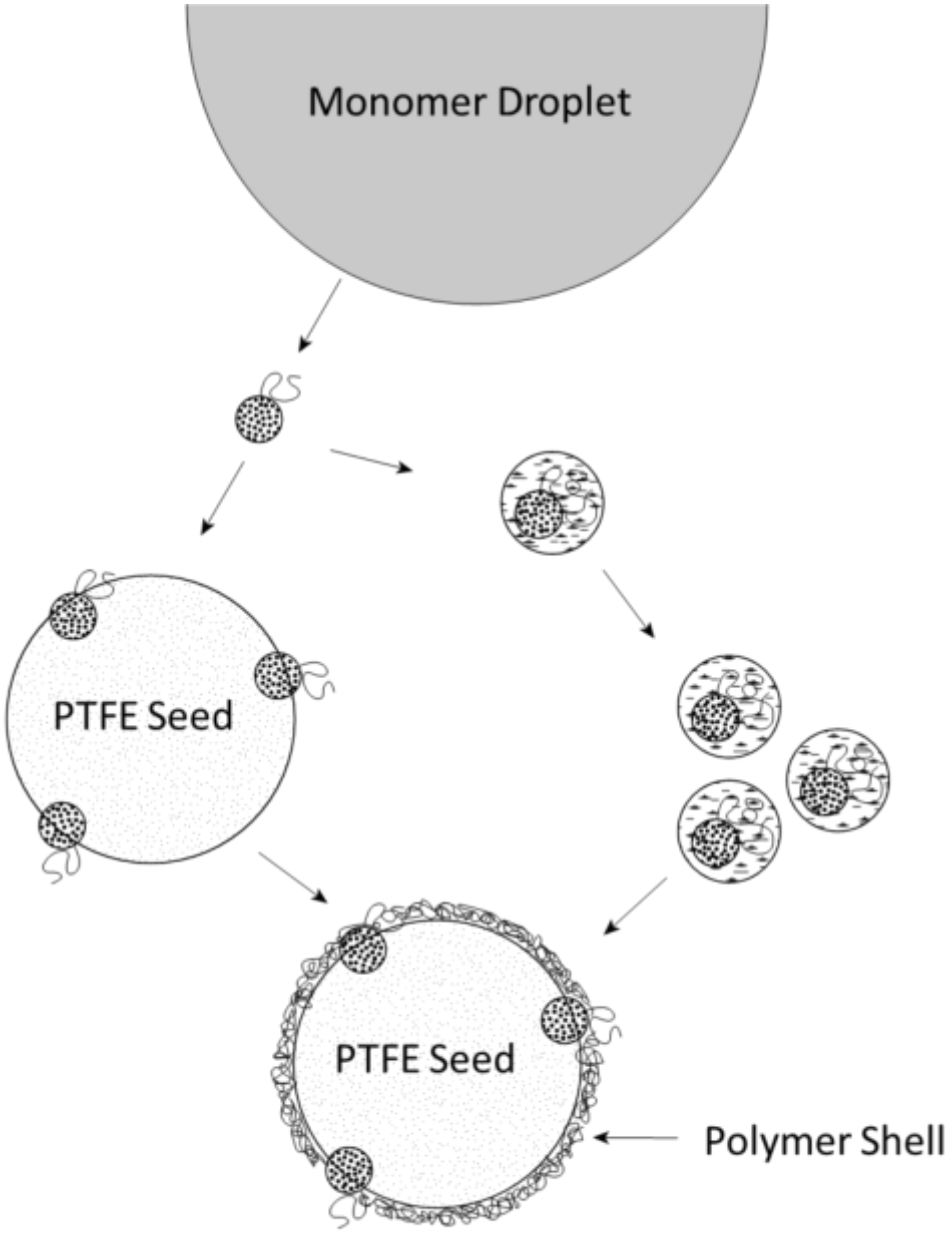

Figure 5. Simplified representation of seeded emulsion polymerization.

A predetermined amount of PTFE was added to 100 mL of water and purged with nitrogen to remove any residual oxygen. Simultaneously the mixture was heated to 75 °C and stirred at a rate of ~250 rpm. Next, MMA, BA, and MAA (all precursors to PMMA) were added according to

Table 5 and the mixture was allowed to dwell at 75 °C for 5 min. Then a 10 mL aqueous potassium persulfate solution (0.075 M) was added. The mixture was kept under a constant flow of nitrogen and was maintained at 75 °C for 24 h. The resulting latex was cooled and stored at room temperature.

Table 5. Recipes for the synthesis of PTFE-PA core-shell particles (MMA=Methyl Methacrylate, BA=Butyl Acrylate, MAA=Methacrylic Acid, KPS=Potassium Persulfate)

Sample	PTFE (g)	MMA (g)	BA (g)	MAA (g)	KPS (g)	DI water (g)
S1	10.0	7.5	2.5	1.0	.20	100
S2	7.0	7.5	2.5	1.0	.20	100
S3	1.8	7.5	2.5	1.0	.20	100

Characterization

The concentration of the PTFE dispersion was determined gravimetrically. Particle size and size distribution were measured by a Horiba LA-950 particle size analyzer. The reported value(s) are the average of five measurements. The instrument was verified by using a known polystyrene standard with diameter of 200 nm. Particle size analysis of the core-shell particles was performed using SEM.

Thermogravimetric analysis (TGA) was performed using a TA Instruments QA50 at a scanning rate of 10 °C/min from room temperature up to 700 °C under nitrogen gas. Differential scanning calorimetry (DSC) was carried out using a TA Instruments Q20 calorimeter. Samples used were approximately 10 mg.

The morphology and dispersion of the composites and PTFE dispersion were observed by scanning electron microscopy (JEOL JSM-6010PLUS-LA). The dielectric permittivity were measured by a Hewlett Packard HP8510C Vector Network Analyzer using a standard WR-90 X-band waveguide as a cavity resonator.

Sample preparation and cavity perturbation measurements

Samples were prepared by spraying the latex onto a heated (70 °C) glass substrate using an ordinary hobby grade airbrush. The glass substrates were first cleaned in acetone while being sonicated for 10 min. The samples were approximately 5.6 mm × 22 mm × 0.15 mm. Prior to spraying the latex onto the substrate, each substrate was weighed and its permittivity measured. 30 samples for each latex composition were fabricated. After spraying the latex, each batch of 30 samples was placed in a vacuum oven for 2 h at 70 °C to remove any remaining water. Each sample was then re-weighed and its permittivity measured.

For the cavity perturbation measurements, a typical WR-90 X-band waveguide was used as the cavity with a small opening machined in the center position of the top of the waveguide. This position coincides with the maximum electric field of the TE_{10N} modes (N = odd). The waveguide, example specimen, and graphical depiction are shown in Figure 6.

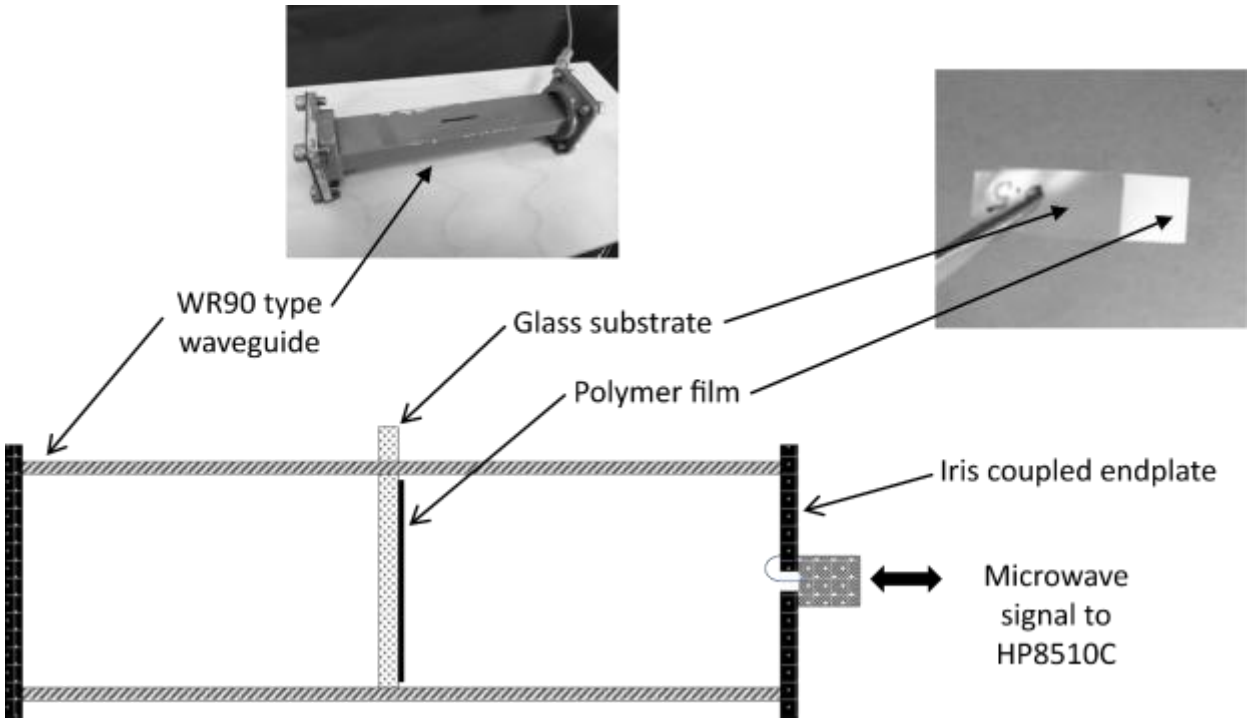

Figure 6. Graphical depiction and photographs of typical experimental setup used in cavity perturbation measurements.

The waveguide was connected to a Hewlett Packard HP8510C Vector Network Analyzer. To measure the thin polymer film properties, first a bare substrate is inserted into the cavity and the resonant frequency and quality factor are recorded. Then once the substrate has been coated with the polymer film, it is inserted into the cavity and again, the resonant frequency and quality factor are recorded. All measurements were taken at 7.2 GHz.

Both real and imaginary parts of the permittivity can be calculated from the changes in the resonant frequencies and Q factors that result when the sample(s) are inserted in the cavity:[13]

$$\varepsilon' = \frac{V_c(f_c - f_s)}{2V_s f_s} + 1 \tag{9}$$

$$\varepsilon'' = \frac{V_c}{4V_s}\left(\frac{1}{Q_s} - \frac{1}{Q'_c}\right) \quad (10)$$

$$Q'_c = Q_c\left[1 + (\varepsilon' - 1)\frac{V_s}{V_c}\right] \quad (11)$$

$$\tan\delta = \frac{\varepsilon''}{\varepsilon'} \quad (12)$$

Where f_c is the frequency of the bare substrate, f_s is the frequency of the substrate and the film, Q_c is the quality factor of the bare substrate, Q_s is the quality factor of the substrate and the film, Q'_c is the quality factor of the film (calculated), V_c is the volume of the empty cavity, and V_s is the volume of the substrate.

3.3. Results and discussion

The dielectric properties of the composites depend not only on the dielectric properties of the individual components, but also other influences including morphology and size of particles, interface interactions, and degree of dispersion of the particles.[23] Consequently, SEM and DSC of the as-purchased aqueous PTFE particles was carried out to understand filler size and morphology, which can be seen in Figure 7. In addition, the PTFE dispersion was annealed at 70 °C for 2 h (also Figure 7). DSC analysis shows that the PTFE particles have a mean size of ~220 nm as seen in Figure 8. Particle size analysis of the core-shell particles using SEM was 417 nm for 10 wt% PTFE, 409 nm for 30 wt%, and 394 nm for 50 wt%.

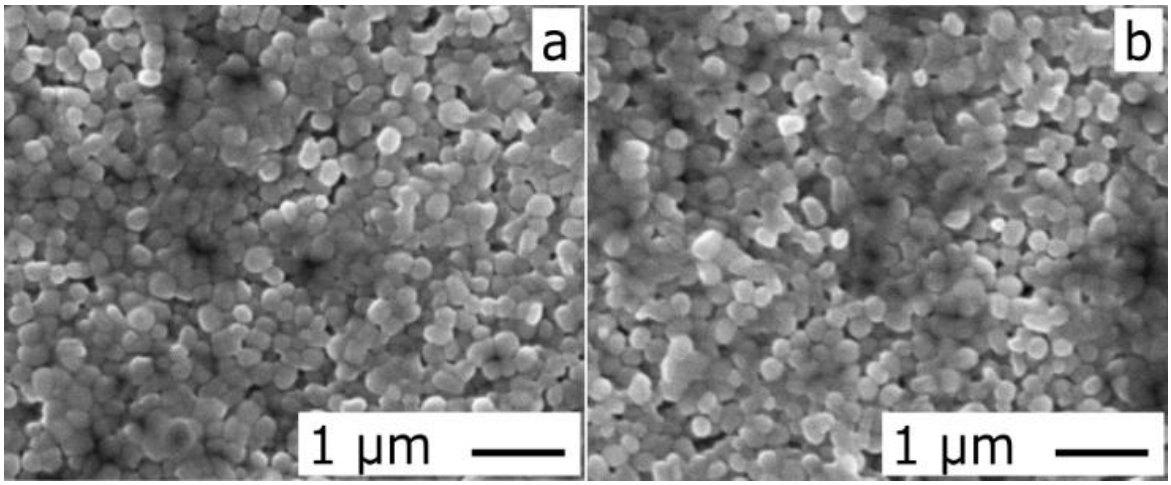

Figure 7. SEM micrographs of as-received PTFE particles dried under vacuum at 30°C (a), and annealed for 2 h under vacuum at 70 °C (b). 10 kV, WD12mm, SS20, ×10,000.

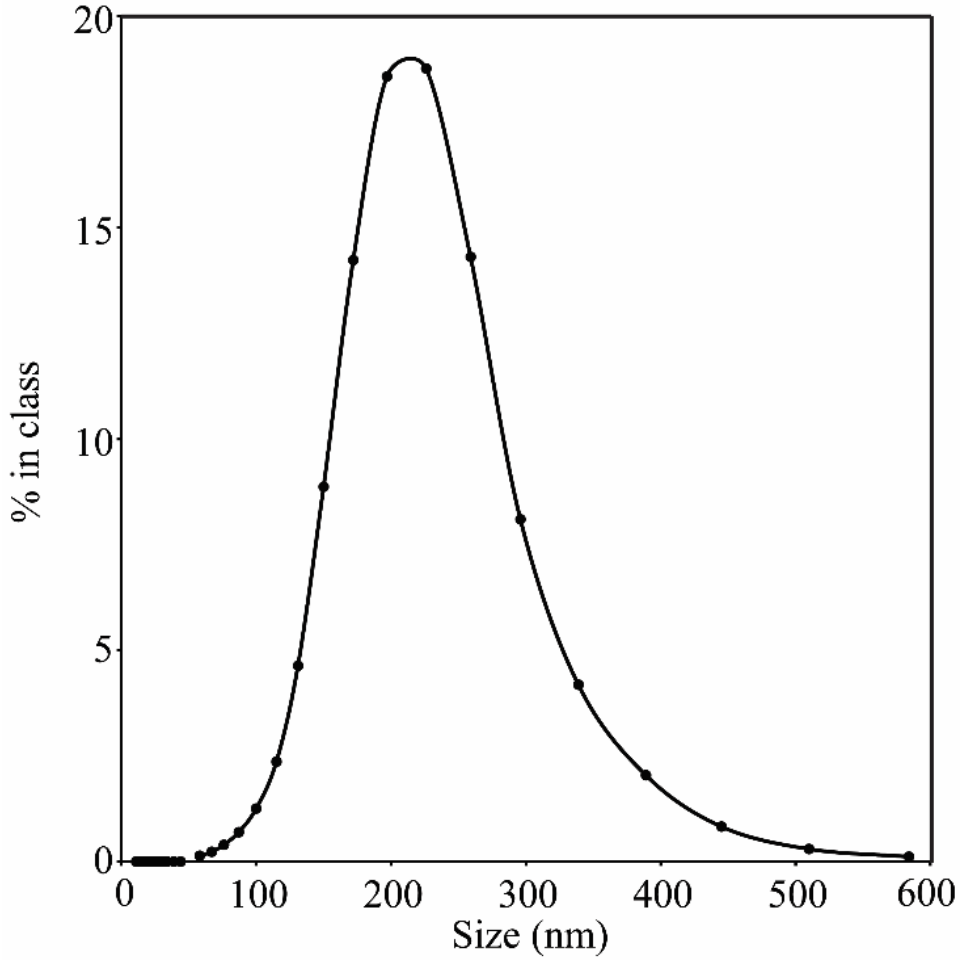

Figure 8. Particle size analysis of the as-received PTFE dispersion.

Figures 9 and 10 report the TGA and DSC heating curves for each core-shell composition. The weight losses at 270 °C and 500 °C clearly belong to PA and PTFE decomposition, respectively. It is clear that the larger nanoparticles correspond to higher PTFE wt%. Similarly, the DSC curves of each composition show an endothermic peak near 325 °C, corresponding to PTFE melting. No clear step due to PA glass transition near 70 °C was observed on DSC curves; however, SEM images revealed PA shell melting at temperatures >70 °C and no melting below 70°C.

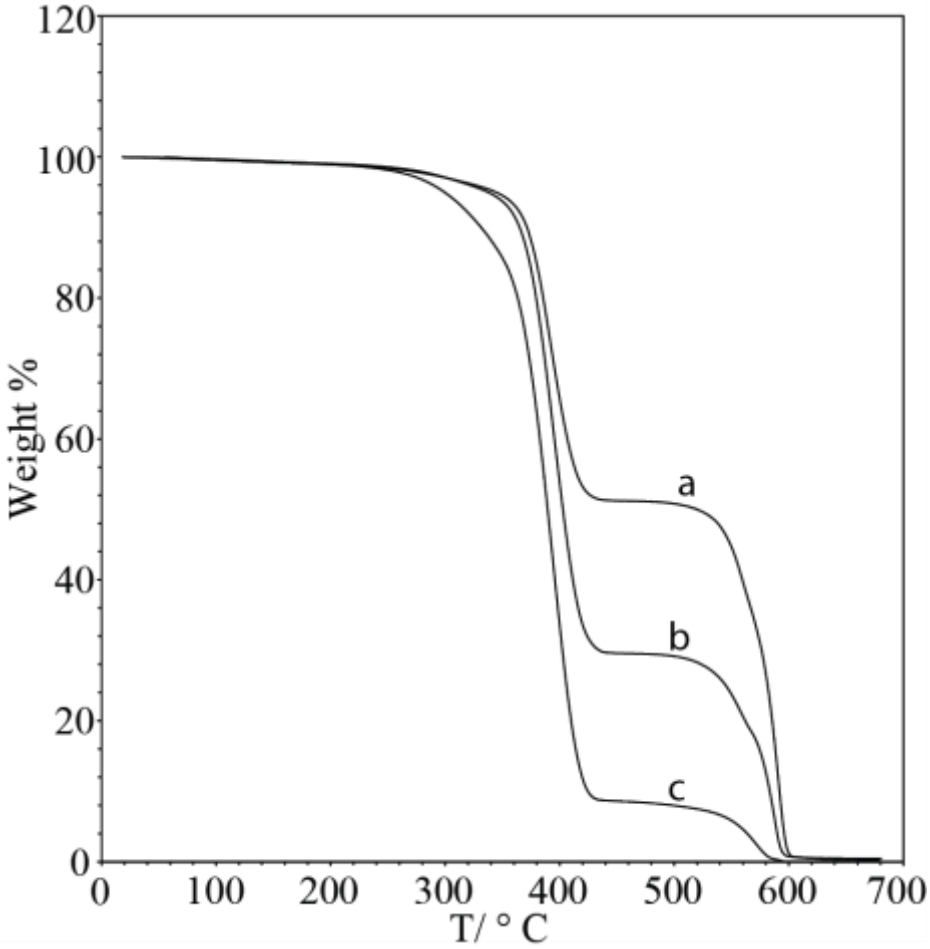

Figure 9. TGA curves at 10 °C/min heating rate for 50 wt% PTFE (a), 30 wt% (b), and 10 wt% (c).

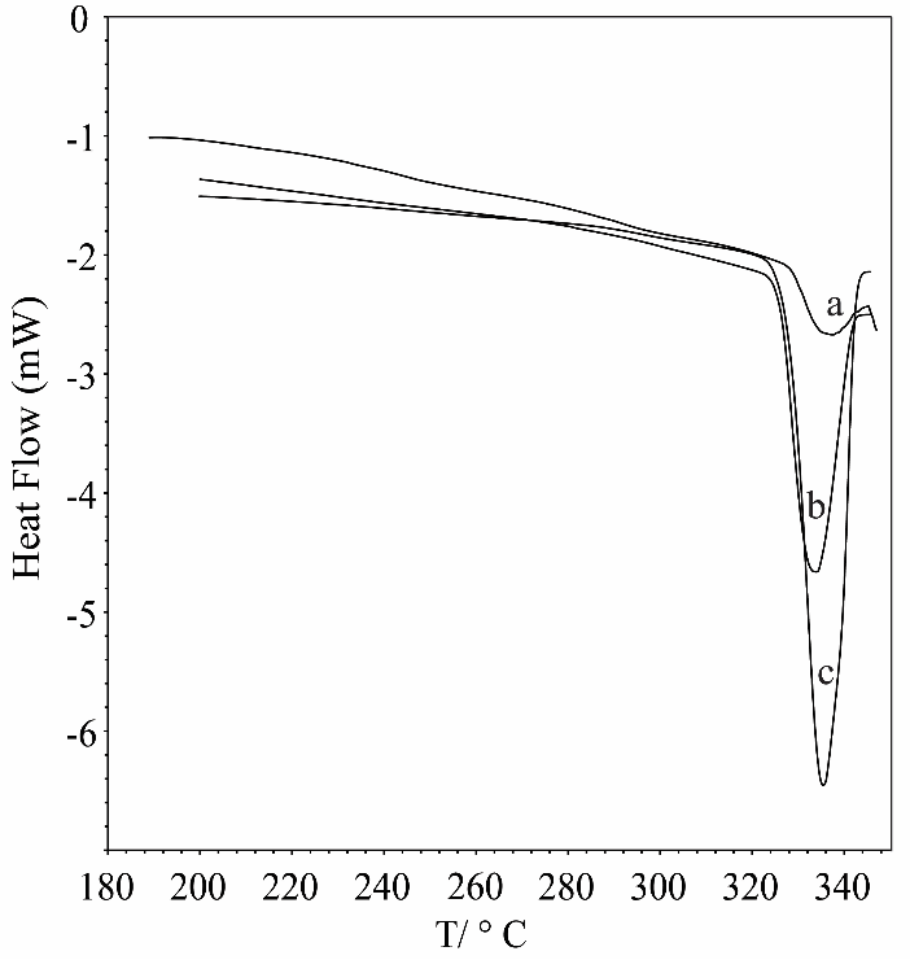

Figure 10. DSC heating curves for 10 wt% PTFE (a), 30 wt% (b), and 50 wt% (c).

Morphologies of the composites and the degree of dispersion of filler in the PA matrix were also studied using SEM. SEM images showing the pre and post annealed films can be seen in Figures 11-13. The images show that as wt% PTFE increases, the percentage of void space increases. The void space was measured and calculated as 10.1% for 50 wt% PTFE, 7.3% for 30 wt%, and 3.9% for 10 wt%. However, even dispersion of the PTFE nanoparticles within the PA matrix is evident.

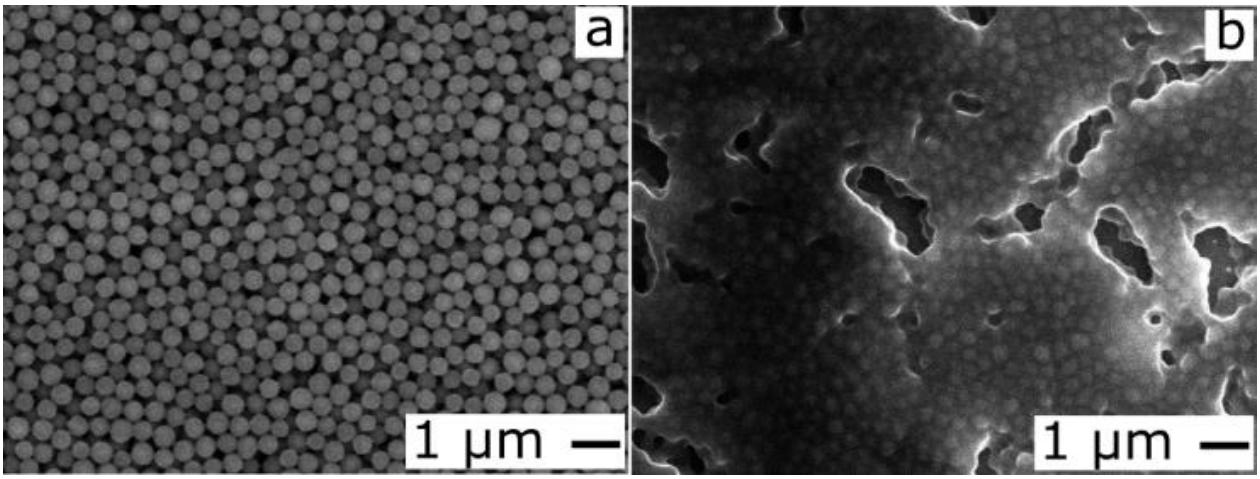

Figure 11. SEM micrograph of a 10 wt% PTFE/PA film dried under vacuum at 30 °C (a), and annealed for 2 h under vacuum at 70 °C (b). 10kV, WD12mm, SS20, ×5,000.

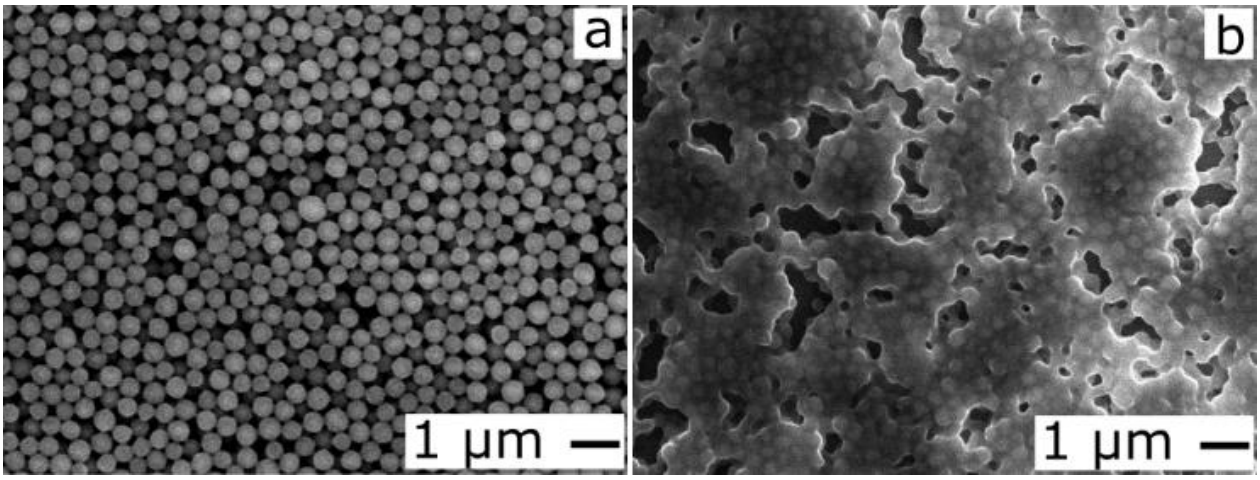

Figure 12. SEM micrograph of a 30 wt% PTFE/PA film dried under vacuum at 30 °C (a), and annealed for 2 h under vacuum at 70 °C (b). 10kV, WD12mm, SS20, ×5,000.

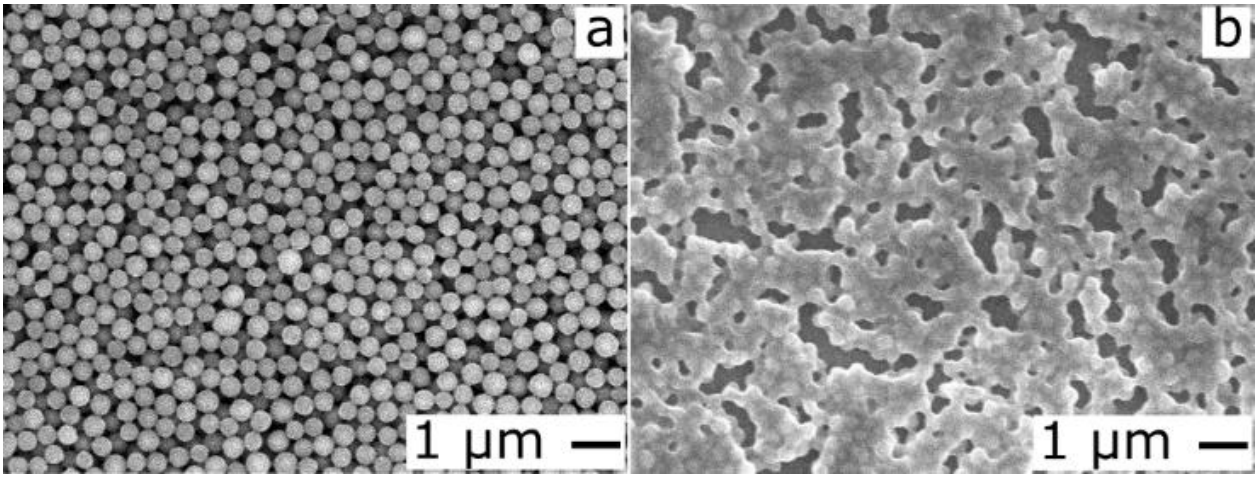

Figure 13. SEM micrograph of a 50 wt% PTFE/PA film dried under vacuum at 30 °C (a), and annealed for 2 h under vacuum at 70 °C (b). 10kV, WD12mm, SS20, ×5,000.

The variation of dielectric constant and loss tangent of the composites as a function of PTFE content can be seen in Figures 14-15. The relative dielectric constant shows a decreasing trend with increasing PTFE content. This is primarily due to the lower relative dielectric constant of PTFE compared with PA. The dielectric constant decreases from 2.63 to 2.33 (± 0.087) as PTFE content increases from 10% to 50%. It can also be seen that the composites have very low loss tangent values. The loss tangent decreases from 3.2×10^{-4}, 2.1×10^{-4} ($\pm 6.7\times10^{-5}$) as PTFE content increases from 10% to 50%.

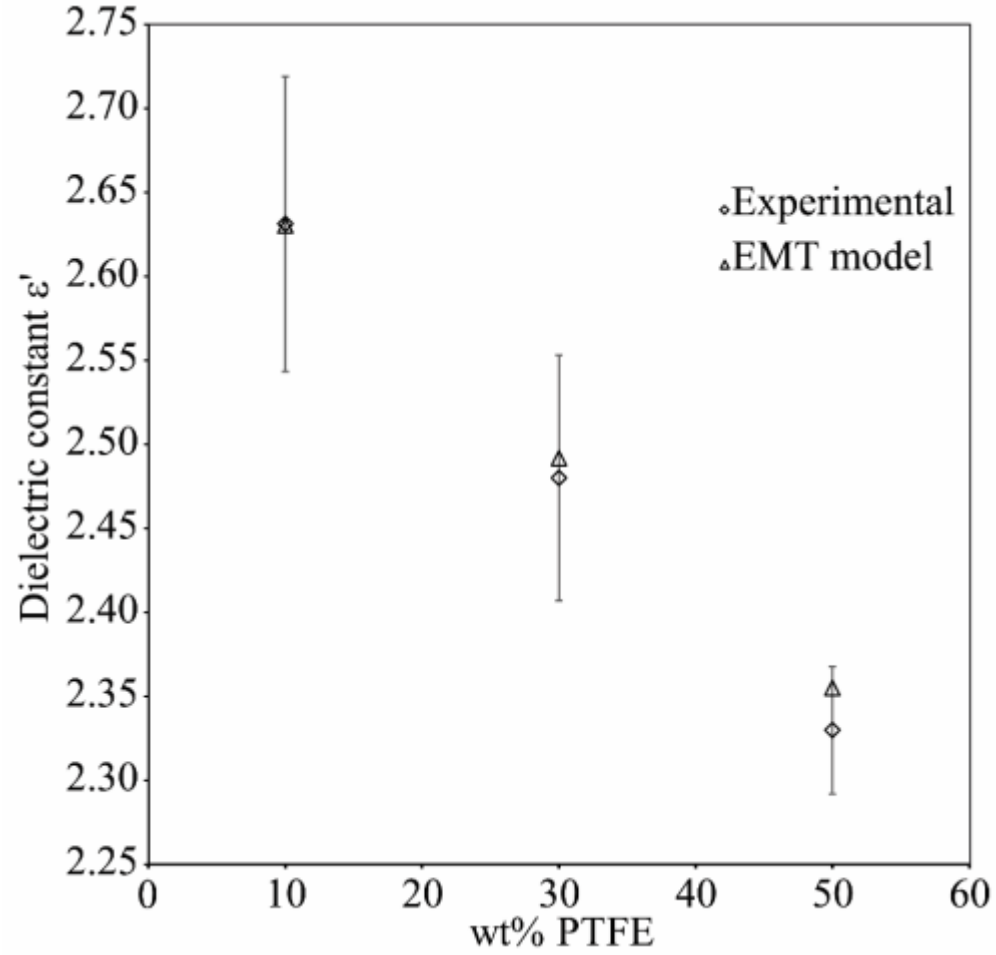

Figure 14. Experimental and calculated dielectric constants of PTFE/PA films using a modified cavity perturbation technique.

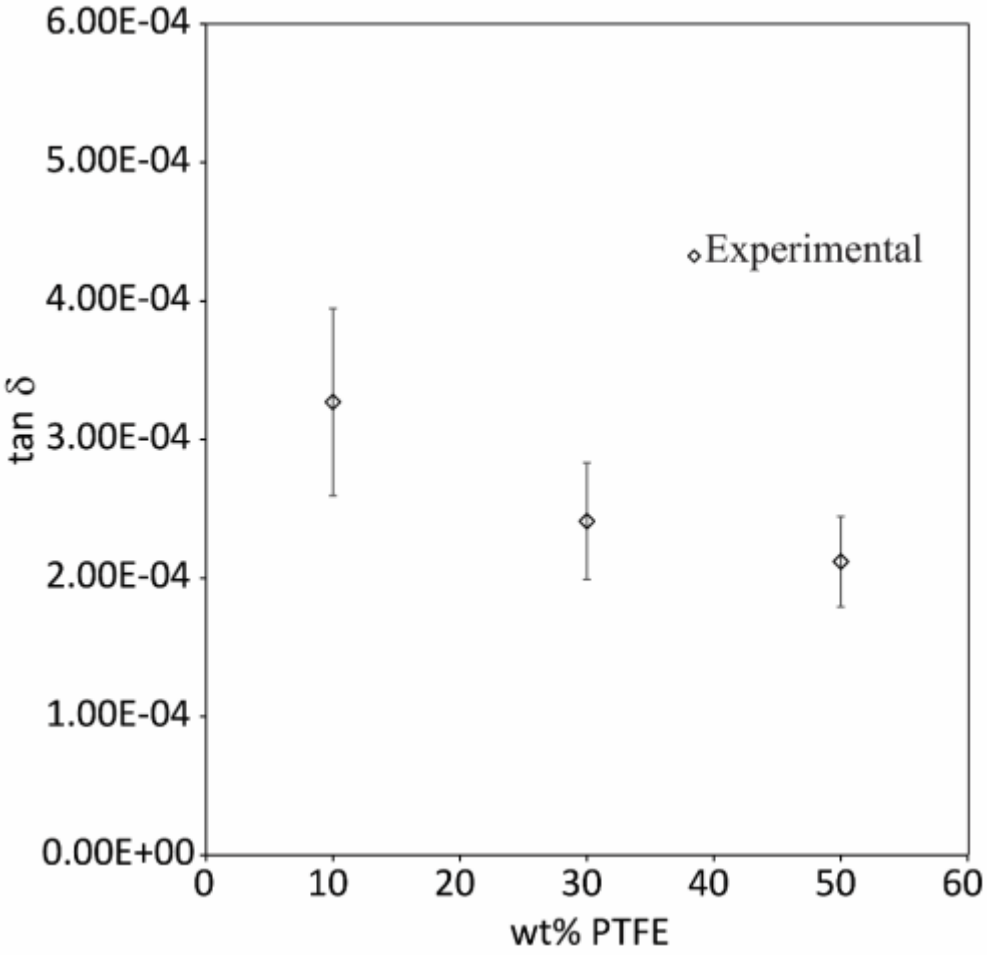

Figure 15. Experimental dielectric loss tangents for PTFE/PA films using a modified cavity perturbation technique.

Several models have been proposed for predicting the effective dielectric constant, including Lichtenecker (Eq. 13),[24] Maxwell-Garnet (Eq. 14),[25] Bruggeman (Eq. 15),[25] and Effective Medium Theory (EMT) (Eq. 16):[26]

$$ln\varepsilon_{eff} = f ln\varepsilon_f + (1-f) ln\varepsilon_m \quad (13)$$

$$\frac{\varepsilon_{eff} - \varepsilon_m}{\varepsilon_{eff} - 2\varepsilon_m} = f\frac{\varepsilon_i - \varepsilon_m}{\varepsilon_i + 2\varepsilon_m} \quad (14)$$

$$f\frac{\varepsilon_i - \varepsilon_{eff}}{\varepsilon_i + 2\varepsilon_{eff}} + (1-f)\frac{\varepsilon_m - \varepsilon_{eff}}{\varepsilon_m + 2\varepsilon_{eff}} \quad (15)$$

$$\varepsilon_{eff} = \varepsilon_m \left[1 + \frac{f(\varepsilon_f - \varepsilon_m)}{\varepsilon_m + n(1-f)(\varepsilon_f - \varepsilon_m)}\right] \quad (16)$$

Where ε_{eff}, ε_f and ε_m are the dielectric constant of the composite, filler and matrix, respectively; f is the volume fraction of filler. The parameter n in Eq. (4) is a fitting factor, which takes on a minimum value as the filler particles become more spherical. Because the Lichtenecker, Maxwell-Garnet, and Bruggeman models do not take into account the interfacial interactions between phases, they are not suitable for predicting the dielectric constant. For the EMT model, when n=0.115 ± 0.005 the confidence interval of the fit is >99% using a χ^2 distribution, as seen in Figure 15. Such a small shape factor indicates a nearly spherical particle, which is in agreement with SEM observations. Hence, in this case, the EMT model is an excellent predictor of the dielectric constant.

The standard error of the measurements is relatively low for the dielectric constant; however, the standard error for the loss tangents is quite high. One reason for this is due to the very small volume of sample. Such a small volume causes only a minute shift in the resonant frequency, therefore the Vector Network Analyzer must have a level of resolution to detect the shift. In addition, a mean film thickness (cross sections measured via SEM) is used to calculate the volume of the sample, which may contain error from the measurement process. In future work, a larger sample volume with more uniform thickness would reduce measurement error.

3.4. Conclusions

PTFE-PA composite films were prepared by aerosol spraying an aqueous dispersion of PTFE-PA core-shell nanoparticles onto a heated glass substrate. SEM observations show a uniform distribution of PTFE particles within a PA matrix. A modified cavity perturbation technique was used to measure the permittivity showing that the dielectric constant decreased with increasing PTFE content and the values were in agreement with those predicted by EMT theory. Hence, aerosol deposition of PTFE-PA core-shell nanoparticles shows that the selection of a shell polymer with the appropriate T_g allows for a viable approach to incorporate PTFE in AM processes. However, further work targeted at decreasing dielectric loss is required; specifically, utilizing shell polymers with lower polarizability than PA should improve the dielectric properties to within acceptable limits for use in microwave devices.

4. Shell polymer optimization: structure-property study

*The majority of this section has been previously published.[27]

4.1. Introduction

Synthesis and development of high performance polymers continues to be a thrust in both academic and commercial research. This is driven by the need for advanced materials supporting a diverse breadth of applications including microelectronics, space, defense, and automotive, to name a few. Often, these applications demand a unique combination of properties. For instance, microwave dielectrics require superlative dielectric properties, good mechanical strength, thermo-oxidative stability, and radiation and solvent resistance.

Polyimides are a class of thermally stable polymers with a research community that continues to grow due to their excellent mechanical, chemical, and electronic properties. The chemistry of polyimides is a vast area of academic interest owing to the myriad monomers available and numerous routes for synthesis. Today, polyimides are used in varied applications including high strength structural adhesives for aerospace, microelectronic interlayer dielectric layers, thin film coatings for optoelectronics, and gas separation membranes.[28] However, due to their chemical inertness and high softening temperatures, their processing can be both difficult and expensive, which limits commercial viability.[29] The most typical processing route entails casting a film of a soluble poly(amic acid) precursor, followed by cyclo-dehydration to render the final imide form. Today's commercial offerings are primarily limited to roll-to-roll processed thick films, where large volume batches are necessary.

Aromatic polyimides have rigid backbone structures and strong interchain interactions, leading to the often poor solubility and non-melting characteristics.[30] Typically, the highly symmetrical and

highly polar groups are responsible for these characteristics. The interchain interactions are derived from the strong intra- and interchain charge transfer complex formation(s) and electronic polarization.[31] The electron accepting imides and electron donating amines support this behavior. Minor variations of either the imides or amines, via subtle variation of the dianhydride and diamine monomers, can yield remarkable alteration on the properties of the polyimide.

Many examples exist in the literature of modifying the properties of polyimides through structural modifications. Typically, polyimide studies involve one of three major structural modifications: 1) introduction of flexible or rigid linkages to the backbone, 2) introduction of bulky (polar or non-polar) substituents, and 3) reduction of symmetry/regularity. For instance, introducing the flexible ether linkage (-O-) puts 'kinks' in the backbone, which reduce rigidity and deter efficient packing of chains.[30] As the distance between chains increases, the chain-to-chain interactions decrease, thereby increasing the solubility. Inefficient chain packing leads to a fractional increase in free volume. It has been shown that free volume contributes to the lowering of the dielectric constant.[8] Bulky substitutes, such as hexafluoroisopropylidene, also reduce packing efficiency by chain distortion. In addition, segmental mobility is greatly hindered causing reduced crystallinity and packing. Again, this leads to a fractional free volume increase. In the case of a fluorine substitution, typically the CF_3 moiety, the C-F bond has decreased polarizability relative to the C-H bond, resulting in overall decreased polarizability of the polyimide. In total, fluorine substitution introduces steric and chemical effects that elucidate the structure-property relationship of polyimides.

Yet despite the numerous studies of structural modifications, currently no studies exist that examine structural modifications and the resulting microwave dielectric properties (7-12 GHz). The aim of this study is to examine the properties that result from introducing: 1) rigid 4,4'-(9-

fluorenylidene) dianiline (FNDA) and 3,3',4,4'-biphenyltetracarboxylic dianhydride (BPDA) segments, 2) flexible 4,4'-(1,3-phenylenedioxy) dianiline (PDODA) segments, and 3) bulky 4,4′-(hexafluoroisopropylidene)diphthalic anhydride. In addition to DSC, TGA, Fourier Transform Infared spectroscopy (FTIR), and dielectric spectroscopy will be used to determine the microwave dielectric properties.

Table 6. Chemical structures and nomenclatures of monomers.

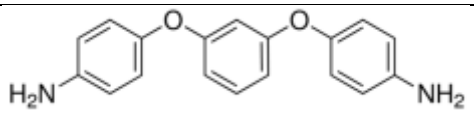	4,4′-(1,3-Phenylenedioxy)dianiline **PDODA**
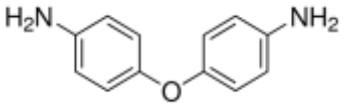	4,4′-Oxydianiline **ODA**
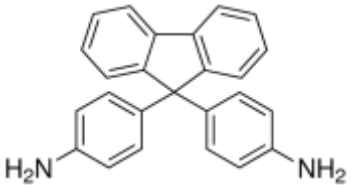	4,4′-(9-Fluorenylidene)dianiline **FNDA**
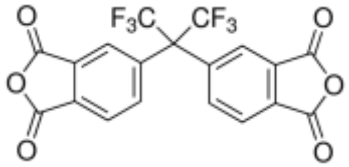	4,4′-(Hexafluoroisopropylidene)diphthalic anhydride **6FDA**
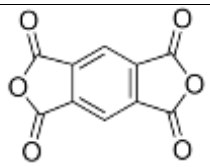	Pyromellitic dianhydride **PMDA**
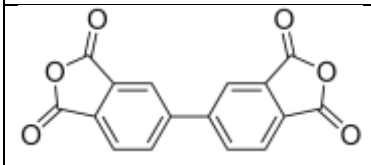	3,3′,4,4′-Biphenyltetracarboxylic dianhydride **BPDA**

4.2. Experimental

Materials and Characterization

The diamines PDODA, ODA, and FNDA and the dianhydrides 6FDA, PMDA, and BPDA were obtained from Sigma-Aldrich. The chemical structures of these monomers can be seen in Table 6. *N*,*N*-Dimethylformamide (DMF) anhydrous 99.8% and triethylamine >99% were also obtained from Sigma-Aldrich.

The thermal properties were investigated by TGA (TA instruments) under an argon atmosphere at a heating rate of 10 °C/min, from room temperature to 750 °C, and DSC (TA instruments) at a heating rate of 10 °C/min, from room temperature to 350 °C. For the DSC analyses, all samples were heated at 200 °C for 30 min to ensure dryness.

Dielectric constants were obtained using cavity perturbation measurements. A typical WR-90 X-band waveguide was used as the cavity with a small opening machined in the center position of the top of the waveguide. This position coincides with the maximum electric field of the TE_{10N} modes (N = odd). The waveguide was connected to a Hewlett Packard HP8510C Vector Network Analyzer.

Samples were prepared by affixing a small sample of polyimide film onto a small strip of Kapton film. Prior to affixing the polyimide film onto the Kapton film substrate, each substrate was weighed and its permittivity measured. 5 samples for each polyimide were fabricated. Each sample was then re-weighed and its permittivity measured. Both real and imaginary parts of the permittivity can be calculated from the changes in the resonant frequencies and Q factors that result when the sample is inserted in the cavity.

Synthesis

The syntheses of the polyimides were performed by the typical two step procedure: synthesis of poly(amic acid) and subsequent thermal imidization as seen in Figure 16.

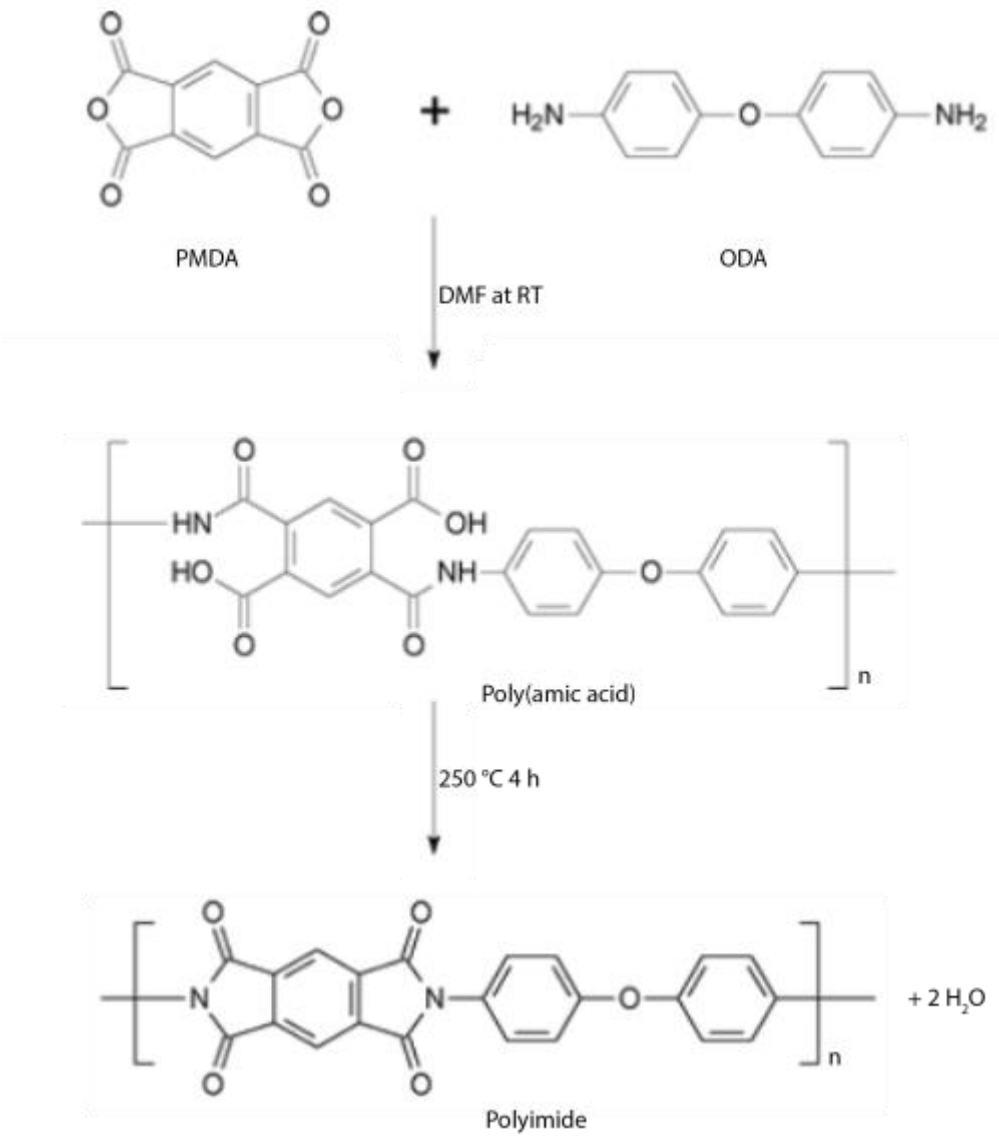

Figure 16. Reaction scheme for a general two step polyimide synthesis.

For the synthesis, equimolar amounts of diamine and dianhydride were dissolved in 10 mL of DMF to form a ~10 wt% solution. Recipes for the polyimides can be seen in Table 7.

Table 7. Recipes for the nine polyimides.

	PMDA (mol)	BPDA (mol)	6FDA (mol)	ODA (mol)	PDODA (mol)	FNDA (mol)	DMF (mL)	yield (%)
PMDA-ODA	0.0025			0.0025			10.00	56
PMDA-PDODA	0.0021				0.0021		10.00	44
PMDA-FNDA	0.0019					0.0019	10.00	63
BPDA-ODA		0.0021		0.0021			10.00	69
BPDA-PDODA		0.0018			0.0018		10.00	71
BPDA-FNDA		0.0016				0.0016	10.00	51
6FDA-ODA			0.0016	0.0016			10.00	48
6FDA-PDODA			0.0014		0.0014		10.00	70
6FDA-FNDA			0.0013			0.0013	10.00	61

The diamine was dissolved first, and then the dianhydride was added as a solid at once. The reaction medium was stirred under a dry N_2 atmosphere at room temperature for 3 h to form the corresponding poly(amic acid). Considerable viscosity increase was observed after 15 min. The poly(amic acid) solutions were precipitated into an excess volume of acetone. The polymers were further washed with ethanol and acetone and then dried under vacuum at 60 ℃ for 24 h. Product yields can be seen in Table 7.

Film Preparation

Films of the polymers were prepared by drop casting 10 wt% poly(amic acid) solutions (50 μL) onto a clean glass plate at room temperature and dried under vacuum at 60 ℃ for 3 h. After this step, the films were removed from the plate and placed inside an oven, which was heated from room temperature to 250 ℃ at 10 ℃/min, and held at 250 ℃ for 3 h. The imidized films were then stored under dry conditions for further characterization. Poly(amic acid) films (no thermal

imidization) were also fabricated and stored for further characterization. Fully imidized films can be seen in Figure 17.

Figure 17. Nine polyimide films: a) PMDA-ODA, b) PMDA-PDODA, c) PMDA-FNDA, d) 6FDA-ODA, e) 6FDA-PDODA, f) 6FDA-FNDA, g) BPDA-ODA, h) BPDA-PDODA, i) BPDA-FNDA.

4.3. Results and discussion

Films of the nine polyimides were drop cast from their poly(amic acid) solutions in DMF and heated to form the polyimides by thermal imidization, followed by removing the solvent under vacuum. All polyimides formed intact, free standing films. FNDA containing polyimides were not creasable, most likely due to the rigid character of the FNDA monomer. The films had characteristic color based on the dianhydride: PMDA polyimides were translucent brown; BPDA

were brownish-yellow with reduced transparency; 6FDA polyimides had little color and greater transparency. Reports confirm the addition of hexafluoroisopropylidene groups typically increases transmittance and can even render colorless films.[32]

Additionally, the structure of the poly(amic acids) and polyimides were investigated by FTIR. An example FTIR spectra for PMDA-PDODA can be seen in Figure 18. A typical FTIR spectrum of polyimide contains two carbonyl peaks related to symmetric and asymmetric stretching, a C-N stretching, and an imide ring. For the PMDA-PDODA polyimide spectrum, these peaks appear at 1777 cm^{-1}, 1713 cm^{-1}, 1374 cm^{-1}, and 721 cm^{-1}, respectively. In contrast, the NH and OH stretch at 3560-3100 cm^{-1}, the C=O stretch at 1640 cm^{-1}, and the C-NH stretching of the amide at 1540 cm^{-1} can be seen in the poly(amic acid) spectra. The interpretation of the FTIR spectra is in agreement with reported values.[29]

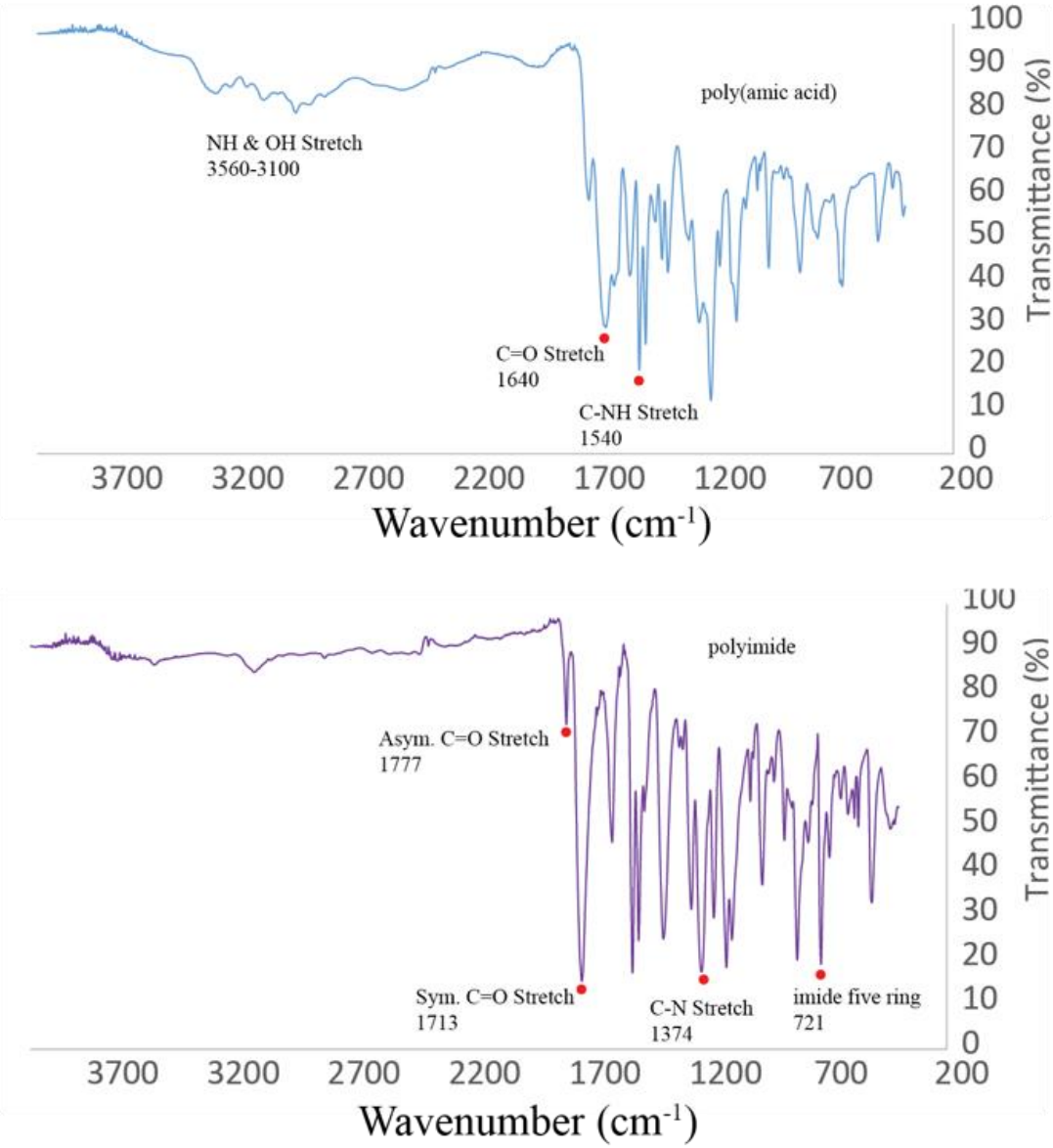

Figure 18. FTIR spectra of PMDA-PDODA poly(amic acid) and polyimide.

The thermal stability of the polyimides was investigated using TGA. Figure 19 shows an example TGA curve for PMDA-ODA at a heating rate of 10 °C/min up to 750 °C. All nine polyimides display degradation temperatures >550 °C. The absence of significant weight loss indicates full imidization of the films and corroborates FTIR data. Additional TGA curves can be seen in Appendix I.

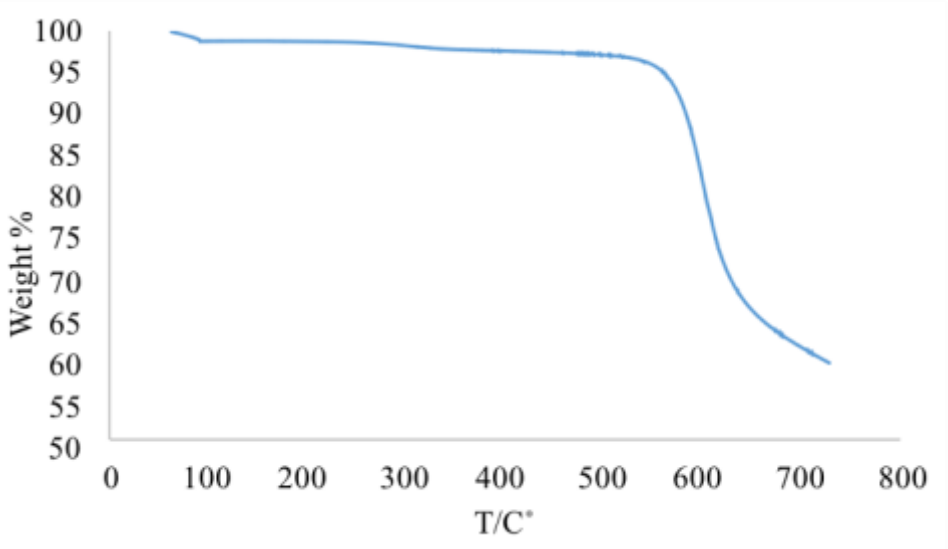

Figure 19. TGA curve for PMDA-ODA polyimide.

The T_g of the polyimides was attempted by DSC. Table 8 lists the T_g and dielectric constants for each polyimide.

Table 8. Glass transition temperatures and dielectric constants for the polyimides.

Polyimide	T_g(°C)	Dielectric Constant (ε')
ODA-PMDA	375	3.65
ODA-6FDA	281	2.84
ODA-BPDA	288	3.42
PDODA-PMDA	300	3.46
PDODA-6FDA	251	2.93
PDODA-BPDA	269	3.54
FNDA-PMDA	-[a]	3.95
FNDA-6FDA	-[a]	3.23
FNDA-BPDA	492[b]	3.71

[a] not observed in DSC. [b] number is taken from the literature

The 6FDA-ODA, 6FDA-PDODA, BPDA-ODA, and BPDA-PDODA containing polyimides show very distinct T_g transitions: 281 °C, 251 °C, 288 °C, and 269 °C, respectively. The DSC heating curves for PMDA-ODA and PMDA-PDODA can be seen in Figure 20. The PMDA-ODA and PMDA-PDODA polyimides show minor transitions at 377 °C and 300 °C, respectively, the former

which agrees well with reported values for PMDA-ODA.[33] No transitions were observed for any FNDA containing polymers. Literature reports a value of 492 °C for BPDA-FNDA,[34] which is well beyond the allowable temperature for the instrument used. These results demonstrate how monomer rigidity/flexibility affects polyimide thermal transitions. The flexible PDODA monomer introduces kinks into the backbone of the polyimide, which in turn reduces the chain packing efficiency and diminishes intermolecular interactions thereby decreasing the T_g. Conversely, the rigid FNDA monomer enables even greater chain packing efficiency, increases the intermolecular interactions and thus the T_g.

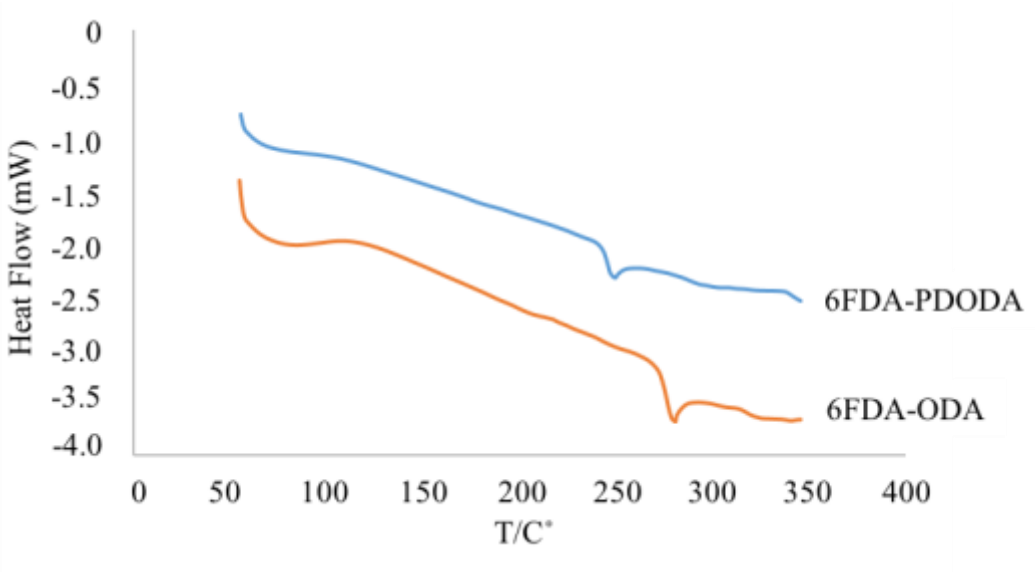

Figure 20. DSC curve for 6FDA-ODA polyimide.

The dielectric constant (ε′) of the polyimide films was measured at frequencies of 7.2, 8.2, and 11.0 GHz. The results can be seen grouped by dianhydride in Figure 21 and grouped by diamine in Figure 22. For a given dianhydride, it is clear that FNDA produces a significant increase in dielectric constant. It is unclear whether this is due to backbone rigidity or the presence of the fluorene group. It is likely that backbone rigidity has a very minor contribution to polarizability, if

any at all. Conversely, backbone rigidity enhances chain packing efficiency. As stated previously, efficient chain packing reduces free volume thereby increasing the dielectric constant. Even though the fluorene group presents steric hindrance for optimal chain packing, the contributions to increasing the dielectric constant from backbone rigidity far exceed the ones from steric effects that lower it. For a given diamine, it is clear that 6FDA produces a significant decrease in dielectric constant. It has been reported that the 6FDA group can have a remarkable effect on dielectric properties of polyimides; specifically, it is known to significantly lower the dielectric constant.[35] Fluorine incorporation influences several properties of polyimides including moisture absorption, thermal stability, and dielectric constant. Moisture absorption is affected by fluorine's hydrophobicity, which makes it difficult for water to absorb onto the surface. Thermal stability is affected *via* steric effects of the CF_3 moiety, which reduces intra- and interchain interactions, thereby reducing the energy required for the onset of molecular motion. A decrease in the dielectric constant benefits from (in addition to hydrophobicity and steric effects) the reduced polarizability of the C-F bond in comparison to the C-H bond. In contrast, there is no clear indication that the flexible PDODA monomer influences dielectric properties. It is expected that this contribution to backbone flexibility would promote inefficient chain packing, leading to an increase in fractional free volume, and thus a lowering of the dielectric constant.

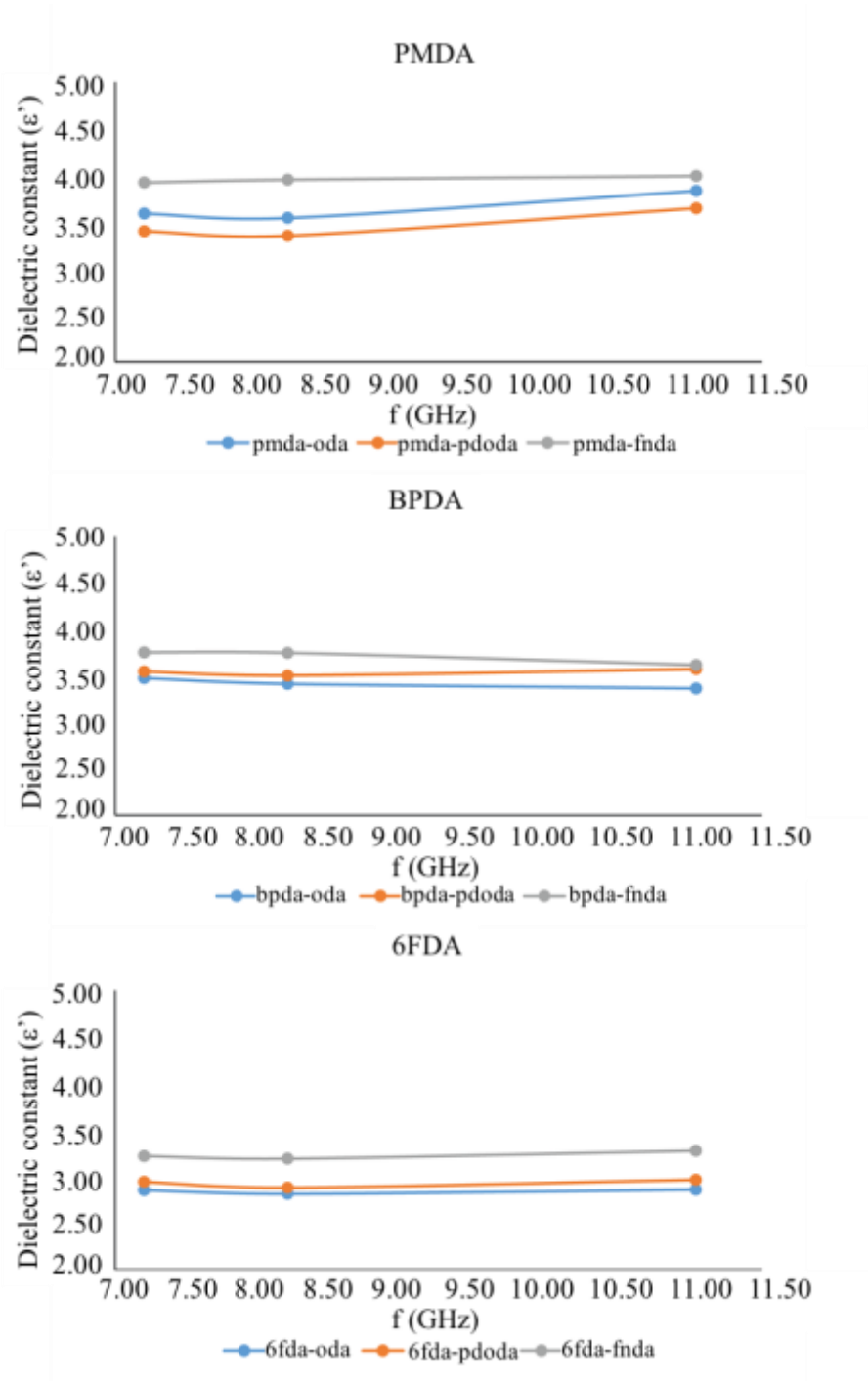

Figure 21. Dielectric constant of polyimides grouped by dianhydride.

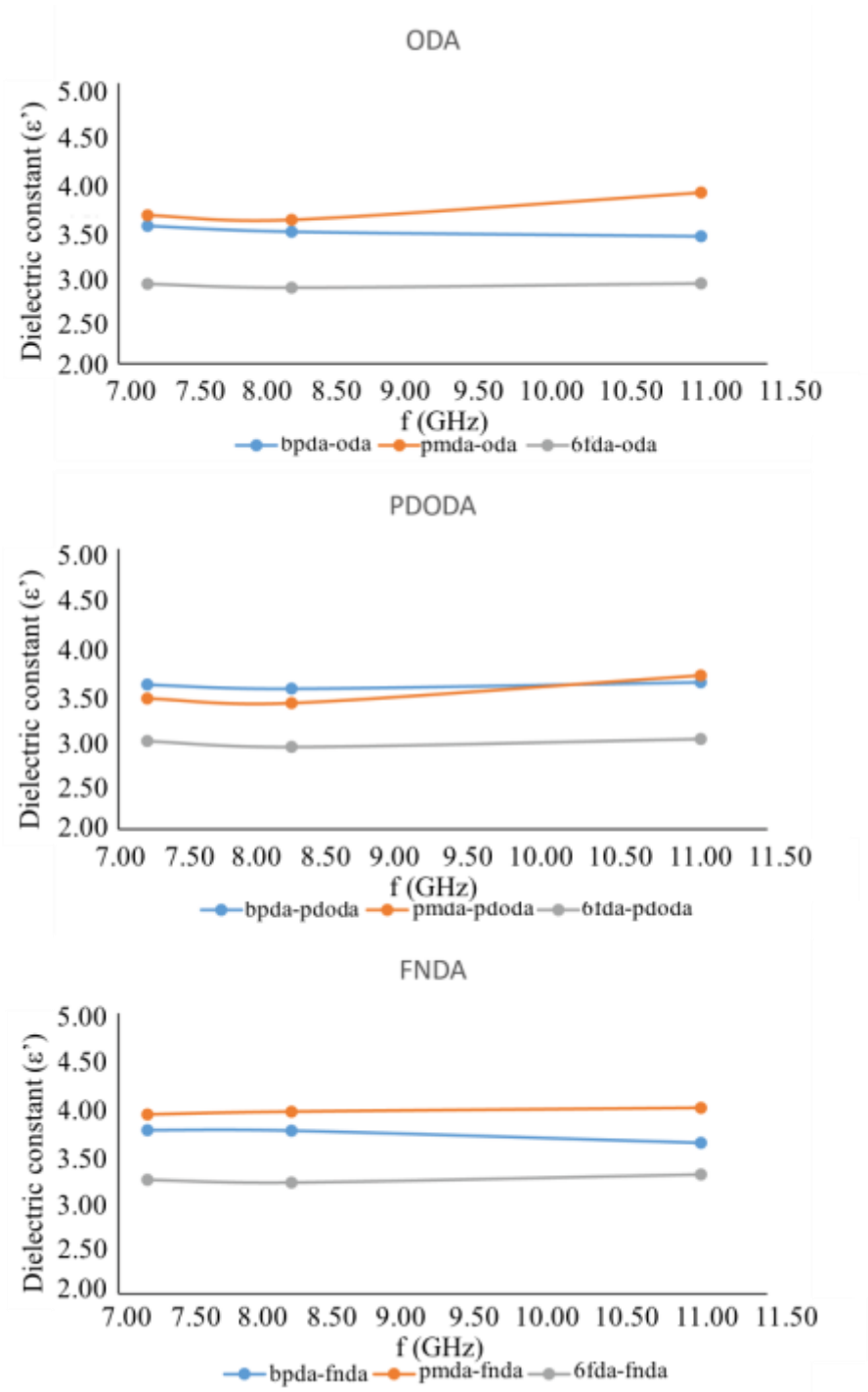

Figure 22. Dielectric constant of polyimides grouped by diamine.

4.4. Conclusions

The influence of major structural modifications on the physical, chemical, and electrical properties of polyimides was investigated. The following conclusions can be drawn: 1) for a given dianhydride, the T_g increases as PDODA>ODA>FNDA, 2) for a given dianhydride, the presence of FNDA increases the dielectric constant by up to 12.4%, 3) for a given diamine, the presence of 6FDA reduces the dielectric constant by up to 22.2%.

The polyimide films characterized in this study have properties equal to or superior to commercially available polyimide films. Specifically, the polyimide 6FDA-ODA produced a tough, creasable film with good thermal properties and very low dielectric constant, making it a promising material for microwave dielectric substrate material.

5. Solution processed low-k dielectric core-shell nanoparticles for additive manufacturing of microwave devices

5.1. Introduction

AM continues to garner attention from manufacturing companies in recent years due to reported advantages of low cost, high quality and reduced waste over traditional subtractive manufacturing.[36-38] Though approaches to replacing traditional subtractive processes with additive ones have been broadly studied by many researchers,[39-42] the most basic substrates, widely made from FR-4 (flame retardant), continue to be made in bulk, off-line and later cut to size. Similarly, substrates for microwave devices made from PTFE are laminate materials made in large batch operations. PTFE, by itself, has never been reported to be used as feedstock in an additive process, largely due to its physical properties, namely its high melt viscosity and low solubility in all common solvents.[43, 44] To realize an additive process for microwave substrate manufacturing, fundamental materials science obstacles must be overcome.

A viable solution is to create a composite material that incorporates additional material(s) capable of surmounting the inherent disadvantage(s) sometimes presented by PTFE. One approach is to use homogeneous multi-phase PTFE containing composites. Xiang et al. reported PTFE/Bi-based composites for microwave use.[45] Thomas et al. reported on PTFE/$ZnAl_2O_4$-TiO_2 and PTFE/$Sm_2Si_2O_7$.[46, 47] More recently, Jin et al. reported on PTFE/$SrTiO_3$ and PTFE/BNT composites for use in RF antennas.[48, 49] While these powder processing techniques have proved useful, it has proven difficult via traditional bulk mixing techniques to achieve sample homogeniety due to the poor adhesion of PTFE particles to the binder matrix, which ultimately manifests a low degree of dispersion.[17] Another approach is to utilize a core-shell structure, in

which individual PTFE particles are encapsulated by other material(s) to form nano-scale particles. Antonioli et al. reported on PTFE/PMMA core-shell nanoparticles for self-assembled opals.[50] This approach will make homogenous dispersion in the bulk automatic.[51] Furthermore, the ratio of components is simply controlled via shell thickness.

Developing a core-shell nanoparticle specifically for the AM of microwave device substrates requires a focus on dielectric properties. Because PTFE has a ε' of 2.1 and *tan* δ less than 0.0001,[13] the shell material(s) used for PTFE based core-shell nanoparticles should have dielectric properties close to PTFE. We previously reported on the viability of aerosol deposition PTFE/polyacrylate (PA) core-shell nanoparticles for microwave substrate manufacturing, achieving a ε' of 2.33 and *tan* δ of 0.00021.[11] However, the PA shell lacks high temperature stability making PTFE/PA core-shell nanoparticles unqualified for commercial use. Polyimides (PI) has been reported to have ε' as low as 2.5 and *tan* δ as low as 0.0015.[29] The use of PI in a core-shell nanoparticle would provide excellent high temperature stability of nanoparticle with minimal influence on the particle's dielectric properties.[52] Therefore, replacing the PA with PI would render a nanoparticle suitable for commercial use. In addition, PI's favorable adhesion characteristics, evidenced by its past wide use as a high performance adhesive,[53] could provide useful in non-contact AM techniques where particle-particle and particle-substrate adhesion is critical.

Herein we discuss a new type of core-shell nanoparticle with PTFE core and PI shell with outstanding thermal stability and excellent microwave dielectric properties that can potentially realize an additive process for microwave substrate manufacturing. A series of PTFE/PI nanoparticles were prepared with different PI shell thickness through the electrostatic interaction between PTFE nanoparticles and poly(amic) acid salt (PAAS, a PI precursor) and was further characterized by FTIR for composition analysis, TEM for nanoparticle shape study and SEM, and

AFM for surface morphology study. In addition to excellent thermal stability from DSC and TGA, results from adhesion testing and dielectric measurements on the aerosol deposited samples were in the range deemed acceptable for microwave device use.

5.2. Experimental

Materials

Monomers 4,4'-(hexafluoroisopropylidene) diphthalic anhydride (6FDA), and 4,4'-oxydianiline (ODA) were purchased from TCI Chemicals; PTFE nanoparticles (60% aqueous dispersion), N-methyl-2-pyrrolidone (NMP), and triethylamine (TEA) were purchased from Sigma-Aldrich. All materials were used as received.

Synthesis of PAAS

PAAS was synthesized using a two-step procedure, involving the synthesis of poly(amic) acid (PAA), followed by conversion to PAAS.[54] Briefly, ODA (0.17 g, 0.82 mmol) in NMP (5 wt%, 4.9 mL) was stirred at 300 rpm for 30 min under a N_2 atmosphere in a 50 mL round-bottom flask, followed by the addition of 6FDA (0.37 g, 0.82 mmol) in NMP solution (5 wt%, 4.9 mL) with continued stirring for 8 h. A 10% molar excess of TEA (0.2 mL) was then added and stirred for 2 h. The solution was added dropwise into acetone (500 mL) to render a solid white precipitate of PAAS.

Synthesis of PTFE/PI Core-Shell Nanoparticles

A series of PTFE/PI core-shell nanoparticles were prepared with different PI shell thickness, controlled by the mass of PI added, as depicted in Table 9. Figure 23 illustrates the synthetic

method. An example is given here to show the synthetic protocol of nanoparticles containing 95 wt% PTFE and 5 wt% PI. A PTFE aqueous dispersion (0.88 g containing 0.53 g PTFE) was first added to de-ionized water (100 mL) in a 250 mL round-bottom flask with stirring at 250 rpm for 10 min. The clear solution was heated to 40 °C and the PAAS (0.028 g) was added and allowed to completely dissolve over a period of 45 min. Stirring at 100 rpm for 8 h yielded a solid suspension. 50 mL quantities of the mixture were added to a PTFE lined autoclave and heated at 150 °C for 12 h to fully imidize the PAAS shell; a 10 mL aliquot was reserved for TEM grid preparation(s). The nanoparticles were centrifuged, re-dispersed in de-ionized water, and centrifuged a final time.

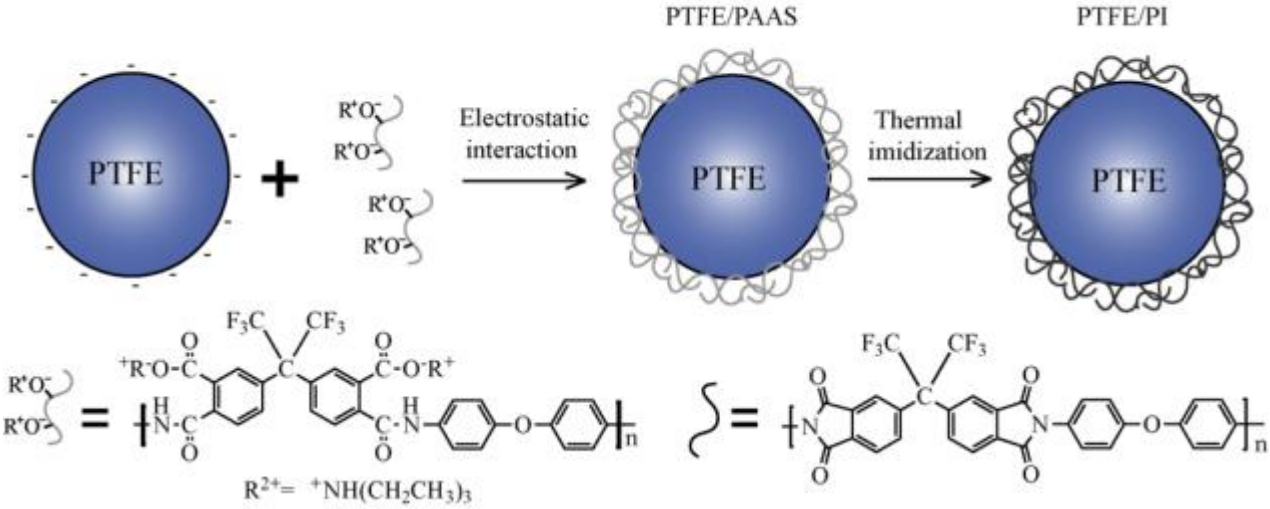

Figure 23. Schematic illustration of self-assembly of PTFE latex particles and PAAS via electronic interaction.

Table 9. Mass of PTFE and PAAS used for synthesis of PTFE/PI core-shell nanoparticles.

Sample (wt%)	PTFE	PAAS
95% PTFE/5% PI	0.53	0.028
90% PTFE/10% PI	0.53	0.053
75% PTFE/25% PI	0.53	0.18
65% PTFE/35% PI	0.53	0.28

Sample Preparation and Characterization

Zeta potential of the PTFE aqueous dispersion was measured using a Zetasizer (NanoZS, Malvern Instruments). Samples for Differential Scanning Calorimetry (DSC, Q200, TA Instruments) and Thermal Gravimetric Analysis (TGA, Q50, TA Instruments) were prepared by drying the centrifuged nanoparticles under vacuum (25 mmHg) at 60 ℃ for 24 h. Both were measured under an N_2 atmosphere at a heating rate of 10 ℃/min. Samples for Fourier Transform Infrared Spectroscopy (FTIR, Bruker Vertex 70 w/ATR), Scanning Electron Microscopy (SEM, Sirion XL30, FEI), and Atomic Force Microscopy (AFM, Bruker Dimension Icon-PT) were prepared by re-dispersing the centrifuged nanoparticles in de-ionized water to make a 5 wt% solution, followed by drop casting onto a sodium borosilicate glass slide and drying under vacuum (25 mmHg) at 60 ℃ for 24 h. Samples for SEM were Au sputtered prior to surface scanning. Samples for Transmission Electron Microscopy (TEM, Technai G2 F20, FEI) were prepared by dispersing 2 drops of a 1 wt% solution onto a carbon coated copper TEM grid (400 mesh) followed by exposure to ruthenium vapors for 1 h. Samples for adhesion testing and dielectric spectroscopy with approximate 2 μm thick were prepared by aerosol spraying a 5 wt% solution onto a sodium borosilicate glass slide heated to 70 ℃. Adhesion characterization was performed using 3M 610 tape in accordance with ASTM F2252. Dielectric spectroscopy was performed at 7.2 GHz utilizing a cavity perturbation technique. The significance for choosing 7.2 GHz in dielectric spectroscopy

is because 1) it falls in range of microwave frequencies, specifically the X-band 7-12 GHz, and 2) the cavity perturbation technique used herein utilizes a waveguide as the cavity resonator and at 7.2 GHz there exists a particularly sharp and well defined resonant peak. Such a sharp, well defined peak is ideal for performing cavity perturbation measurements. For the cavity perturbation measurements, a typical WR-90 X-band waveguide was used as the cavity with a small opening machined in the center position of the top of the waveguide. This position coincides with the maximum electric field of the TE_{10N} modes (N = odd). The waveguide was connected to a Hewlett Packard HP8510C Vector Network Analyzer. To measure the thin polymer film properties, first a bare substrate is inserted into the cavity and the f_c and Q_c are recorded. Then once the substrate has been coated with the polymer film, it is inserted into the cavity and again, the f_s and Q_s are recorded.

Both ε' and ε'' can be calculated from the changes in the resonant frequencies (i.e. f_c and f_s) and quality factors (i.e. Q_c and Q_s) that result when the sample is inserted in the cavity:[55, 56]

$$\varepsilon' = \frac{V_c(f_c - f_s)}{2V_s f_s} + 1 \tag{17}$$

$$\varepsilon'' = \frac{V_c}{4V_s}\left(\frac{1}{Q_s} - \frac{1}{Q'_c}\right) \tag{18}$$

$$Q'_c = Q_c\left[1 + (\varepsilon' - 1)\frac{V_s}{V_c}\right] \tag{19}$$

$$tan\,\delta = \frac{\varepsilon''}{\varepsilon'} \tag{20}$$

5.3. Results and discussion

Material Synthesis

The preparation of a PTFE/PI core-shell nanoparticle *via* self-assembly of PTFE nanoparticle and PAAS followed by thermal imidization is shown in Figure 23. The zeta potential of PTFE aqueous dispersion was -37.2 mV, suggesting that the PTFE nanoparticles were highly negatively charged. In contrast, the PAAS is known to be slightly positively charged due to the presence of the quaternary ammonium groups.[57] The negative and positive potential create coulombic attraction between the PTFE and PAAS, enabling the reaction through electrostatic interaction. After careful addition of PAAS to the PTFE aqueous dispersion, particle coagulation was observed, indicating that the PAAS had self-assembled onto the PTFE nanoparticles through electrostatic interaction. This was further confirmed after thermal imidization and centrifugation, when the clear supernatant was poured into excess acetone, revealing no precipitation, thus indicating complete assembly of PAAS onto PTFE. Our later FTIR analysis (discussed in next section, Figure 24) proved the successful incorporation of PI with PTFE to form PTFE/PI composites while further microscopic study using TEM (discussed later, Figure 3) proved that the PTFE/PI composite do in fact possess a core-shell structure. A facile synthesis such as this is favorable for AM for several reasons: 1) an aqueous medium with little or no remnants of reactant chemicals is typically non-toxic and requires only modest heat to drive off moisture following non-contact deposition such as aerosol or inkjet printing; 2) the synthesis reaction is not complex and requires no special equipment other than modest heat; and 3) the synthesis scales easily to produce large quantities suitable for commercial use.

FTIR Analysis

To prove that the PI had been successfully incorporated with PTFE, FTIR analysis was conducted on the synthesized composite, which is shown in Figure 24. A 100% PAAS spectrum is shown as a baseline prior to thermal imidization. The spectrum clearly shows the characteristic absorption peaks of PAAS at 1656, 1546, and 1404 cm^{-1}, attributed to the C=O of the amide, the amide C-NH bend, and C=O of –COOH, respectively. The 75% PTFE/25% PI spectrum shows the new characteristic absorption peaks of PI. The presence of peaks at 1786, 1720, 1375, and 725 cm^{-1} can be attributed to the asymmetric C=O stretch, symmetric C=O stretch, C-N stretch, and imide ring deformation, respectively. The 75% PTFE/25% PI spectrum also clearly shows the characteristic absorption peaks of PTFE at 1202 and 1145 cm^{-1}, attributed to the C-F stretch. FTIR analysis shows that the imide ring formation occurred to completion following thermal imidization as revealed by the complete disappearance of the C=O amide peak (1656 cm^{-1}) and C-NH bend peak (1546 cm^{-1}), and the appearance of the imide ring peak (725 cm^{-1}).

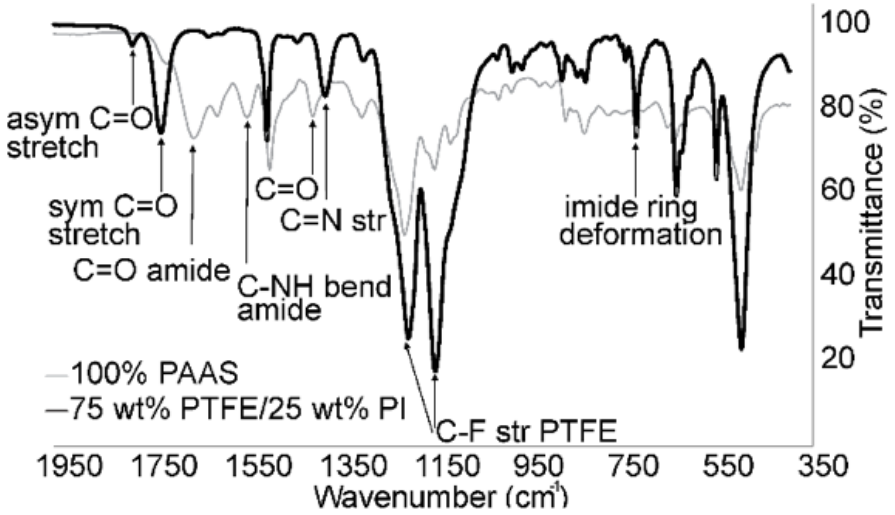

Figure 24. FTIR analysis of PAAS and PTFE/PI core-shell nanoparticles.

Microscopy Study

Compared to the FTIR analysis which only provides information on the incorporation of PI to PTFE after synthesis, images of the composites obtained from TEM and SEM provides critical information, suggesting that the PTFE/PI composites have a core-shell structure. The shape and morphology of the synthesized materials were characterized by TEM and SEM, respectively and can be seen in Figure 25. TEM images shown in Figures 25A (90% PTFE/10 % PI) and B (75% PTFE/ 25% PI) clearly show that the PTFE nanoparticles become encapsulated within the PI shells. A thicker PI shell in 75% PTFE/25 % PI nanoparticle sample (22 nm compared to 9 nm for the 90% PTFE/10 % PI nanoparticle sample) is consistent with the material synthesis protocols that the thickness of the PI shell is controlled by the amount of PI added into the reaction. These TEM images also do not show the presence of any void space between the core(s) and shell(s), indicating a strong interaction between PTFE and PI. A strong coupling between the core and shell is important when considering the bulk dispersion of PTFE amongst PI; when the coupling is strong and no separation of the shell from the core occurs, a homogeneous dispersion can be formed provided the shell thickness from particle to particle is uniform. Poor dispersion leads to non-uniform properties, which is undesirable for microwave substrates.

Morphology of a drop cast film, in the form of SEM and AFM images, of PTFE nanoparticles, 90% PTFE/10% PAAS core-shell nanoparticles, and 90% PTFE/10% PI core-shell nanoparticles can be seen in Figures 25C-E and Figures 26A-C. PTFE nanoparticles are approximately 200 nm as seen in Figure 25C. Figures 25D and E clearly show individual PTFE particles residing in the PAAS and PI matrix, respectively, after the introduction of PAAS followed by thermal imidization on a hot plate at 150 °C for 15 min. Upon careful examination, one can see that the PAAS shells coalesce and form a more continuous matrix once imidized to PI while there remains appreciable

porosity between individual particles within the film. Indeed, some porosity and free volume between polymer chains is desirable when it is homogeneous throughout the solid due to its effective lowering of the ε' because of the low ε' of air (ε' = 1);[58] The more porous, the more surface area the nanoparticles have; however, porosity encountered on external boundaries (i.e. surfaces) will increase the chance of water absorption, which is highly undesirable because water absorption contributes to an increase in the ε' because of the high ε' of water (ε' = 80).[59] The formation of a continuous PI matrix after thermal imidization of PAAS reduces the porosity on external boundaries and thus can help to decrease the water absorption. This is further supported by the surface roughness measurements by AFM. A reduction of the surface roughness is clearly observed in the AFM image of 90% PTFE/10% PI (Figure 26c) compare to PTFE, 90% PTFE/10% PAAS (Figure 26b) and PTFE (Figure 26c). The Root Mean Square (RMS) values obtained from surface roughness measurements for PTFE, 90% PTFE/10% PAAS, and 90% PTFE/10% PI are 58 nm, 59 nm, and 49 nm, respectively. The combination of remnant porosity within the film and decreased surface roughness provided a low ε' film upon imidization (discussed later in Figure 28).

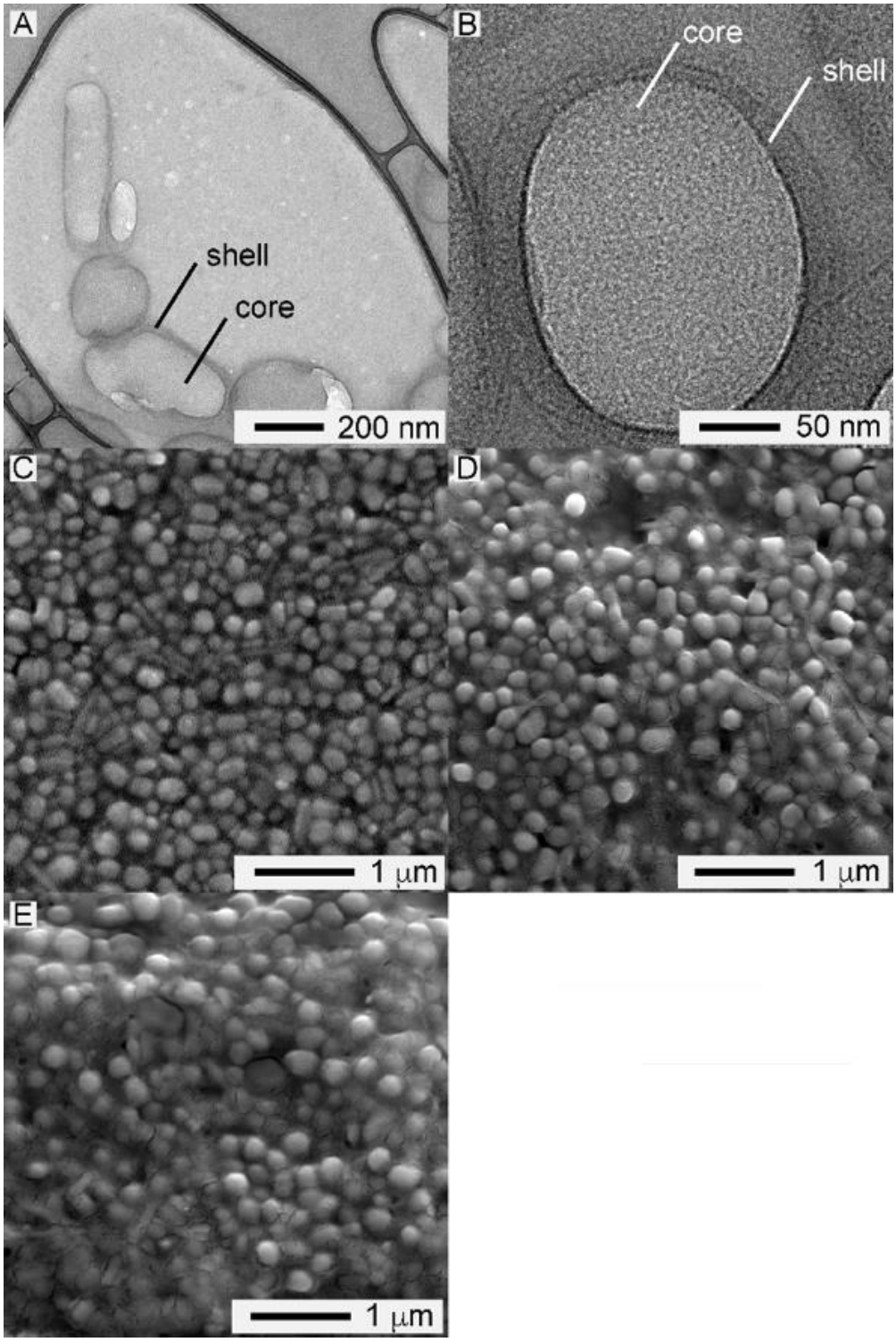

Figure 25. TEM images of A) 90% PTFE/10 % PI core-shell nanoparticles and (B) a 75% PTFE/ 25% PI core-shell nanoparticle; SEM images of (C) as-received PTFE particle, (D) 90% PTFE/ 10% PAAS core-shell nanoparticles, and (E) 90% PTFE/ 10% PI core-shell nanoparticles.

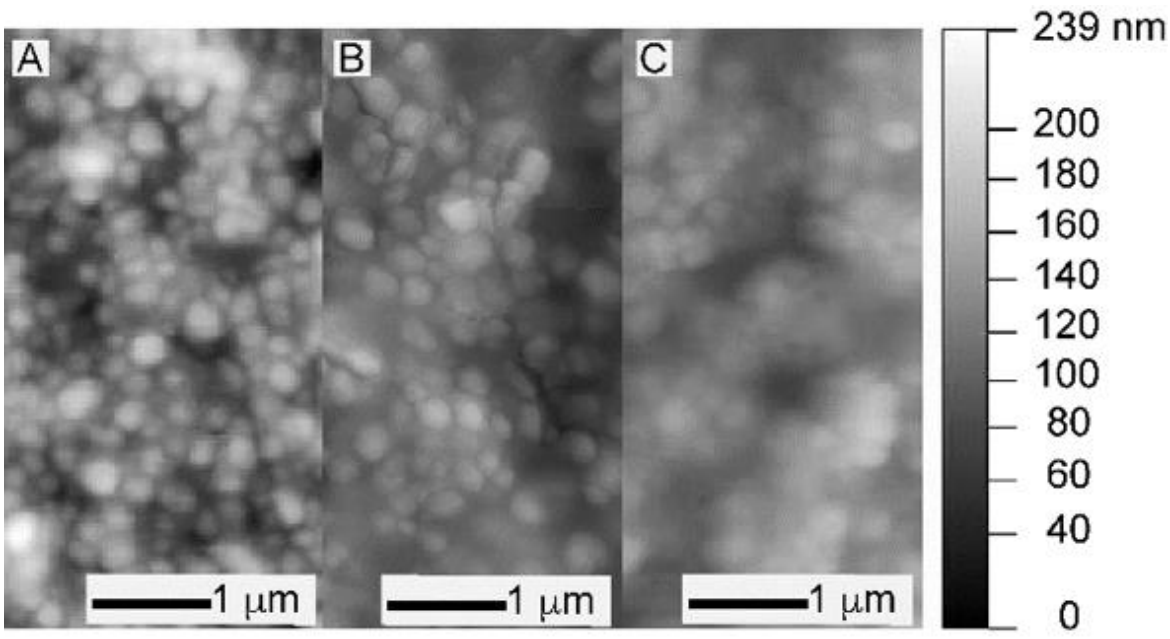

Figure 26. AFM images of (A) as-received PTFE particles, (B) 90% PTFE/ 10% PAAS core-shell nanoparticles, and (C) 90% PTFE/ 10% PI core-shell nanoparticles.

Properties of Nanoparticles

After characterizing the PTFE/PI core-shell nanoparticle in terms of PI incorporation, nanoparticle shape and surface morphology, the PTFE/PI core-shell nanoparticles were characterized for their thermal, adhesion and dielectric properties, as they pertain to AM. The thermal properties of PTFE/PI core-shell nanoparticles were examined using DSC and TGA, as seen in Figure 27. The DSC curves for all wt%s clearly show the characteristic PTFE endotherm near 330 °C, as reported elsewhere.[60] The magnitude of the endotherm increases with increasing wt% PI (or decreasing wt% PTFE) indicating that the endothermic enthalpy of PI is higher than PTFE. The thermal stability of all wt%s can also be seen in Figure 27. The decomposition temperature (defined as 5% of total weight loss) decreases slightly 528 °C to 524 °C as the wt% PI increases compared to 100% PTFE (535 °C). This slight reduction in thermal stability of the PTFE/PI core-shell

nanoparticles can be attributed to the markedly lower thermal conductivity of PI (0.00524 W/mK) versus that of PTFE (0.25 W/mK).[61] It is believed that the lower thermal conductivity of PI impedes the release of heat from the external surfaces, trapping interior heat which results in an earlier decomposition temperature. Even so, the thermal properties of PTFE/PI core-shell nanoparticles are improved compared to our previously reported PTFE/PA core-shell nanoparticles.

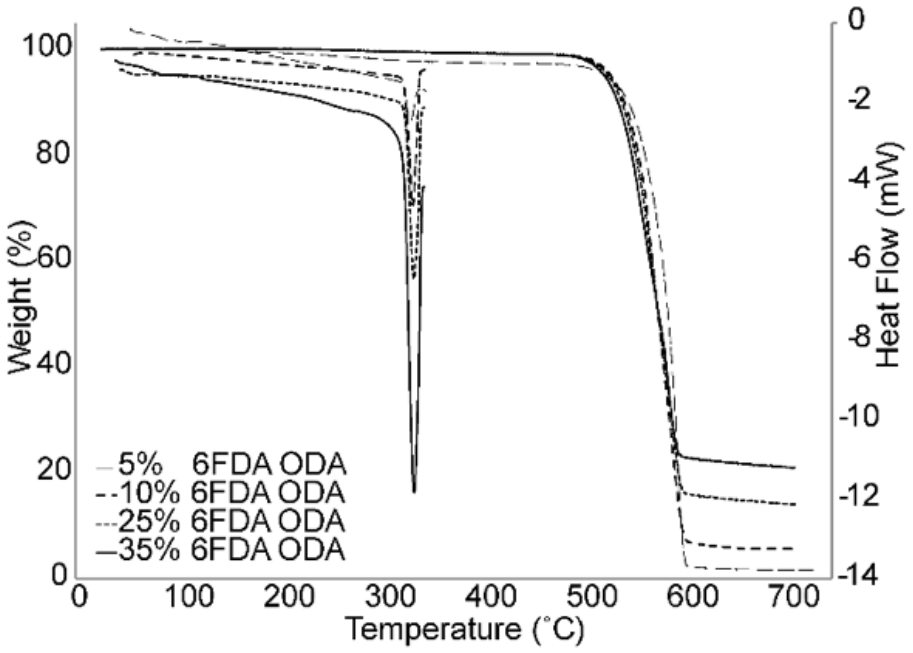

Figure 27. DSC curves and TGA curves for different wt% PTFE/PI core-shell nanoparticles.

The adhesion properties of aerosol sprayed samples were characterized using a tape test in accordance with ASTM F2252-03 Standard Practice for Evaluating Ink or Coating Adhesion to Flexible Packaging Materials Using Tape.[62] In this method, the external force is applied by the thumb or forefinger (no specified force value is provided) along the tape to make sure it is fully adhered, without any bubbles in surface. Good adhesion is particularly important for non-contact deposition processes to ensure longevity and durability of the material once deposited onto the

build substrate. Five samples were prepared for each wt%, including 100% PTFE. Results are reported in Table 10. 100% PTFE failed all five trials, while each wt% PI sample passed a minimum of 3/5 trials. The ability to provide substrate adhesion and particle to particle adhesion is due to the presence of the PI shell. PI has long been utilized across multiple industries as a high performance structural adhesive,[63] thus it is expected that at even small wt% PI content, significant improvement in adhesion would be observed.

Table 10. Results for adhesion testing in accordance with ASTM F2252-03.

Sample	Trial #1	Trial #2	Trial #3	Trial #4	Trial #5	Overall
100% PTFE	-	-	-	-	-	0/5
95% PTFE/5% PI	-	+	+	+	-	3/5
90% PTFE/10% PI	+	+	+	-	+	4/5
75% PTFE/25% PI	+	+	-	+	-	3/5
65% PTFE/35% PI	-	-	+	+	+	3/5

To investigate the dielectric properties (ε' and $tan\ \delta$) of the core-shell nanoparticles, individual ε' values of PTFE, PAAS and PI were first measured and were found to be 2.1, 6.92 and 2.84, respectively. Note that the ε' value of PAAS are much higher than that of PI due to the ionic nature of the salt. Therefore, it is expected that a higher ε' value will be observed for PTFE/PASS core-shell nanoparticles than for PTFE/PI core-shell nanoparticles. As shown in Figure 28A, the measured ε' values of PTFE/PAAS core-shell nanoparticles are all higher than those of PTFE/PI core-shell nanoparticles confirming our expectation.

Figure 28A also shows that the measured ε' values agree well with Effective Medium Theory (EMT), which models how ε' values change with composite composition. We previously reported on EMT and its applicability to core-shell architecture(s) when modeling dielectric properties.[64] The equation describing EMT is:

$$\varepsilon_{eff} = \varepsilon_m \left[1 + \frac{f(\varepsilon_f - \varepsilon_m)}{\varepsilon_m + n(1-f)(\varepsilon_f - \varepsilon_m)}\right] \quad (21)$$

Figure 28A shows that the increase of the PAAS and PI content in PTFE (5 wt% to 35 wt%), increases *ε'* values of both PTFE/PAAS core-shell nanoparticles (from 2.30 to 3.58) and PTFE/PI core-shell nanoparticles (from 2.14 to 2.38).

In addition to *ε'*, *tan δ* values for the core-shell nanoparticles were measured. It is noted in Figure 28B that different from *ε'*, the standard error of which is relatively low, the standard error for *tan δ* are quite high. One reason for the large tan δ standard error is due to the very small volume of sample. Such a small volume causes only a minute shift in the resonant frequency, therefore the Vector Network Analyzer must have a level of resolution to detect the shift. Nevertheless, the observed trend on *tan δ* values of PTFE/PI core-shell nanoparticles is similar to their *ε'* values, showing an increasing trend with increasing PI content. Additionally, as expected, the *tan δ* values of PTFE/PAAS core-shell nanoparticles are higher than those of PTFE/PI core-shell nanoparticles. Ultimately, the 5 wt% PI composite film provided the best dielectric properties out of the spray coated films in our study where *ε'* = 2.14 and *tan δ* = 0.001, which are suitable values for commercial applications.

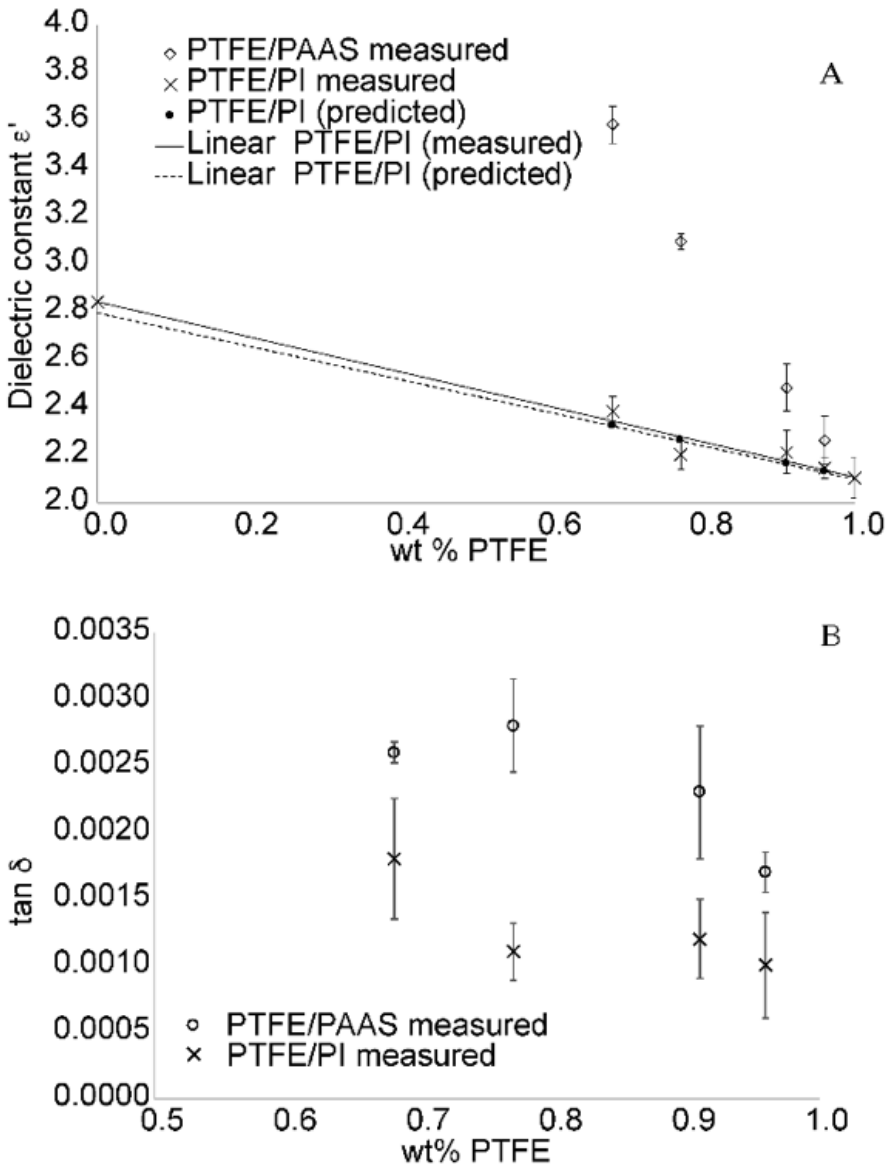

Figure 28. Measured and predicted (A) *ε'* and (B) *tan δ* for various wt% PTFE/PAAS and PTFE/PI core-shell nanoparticles. Note: The *ε'* for 100% PTFE was measured using a commercially available PTFE film 5 μm in thickness.

5.4. Conclusions

A simple approach for preparing a low-k dielectric PTFE/PI core-shell nanoparticle by self-assembly of PTFE nanoparticles and PAAS through electrostatic interaction, followed by thermal

imidization, is reported. The core-shell structure was characterized by FTIR and confirmed by TEM. SEM and AFM studies indicated that a porous material network with a smooth and continuous PI matrix on the surface, which helps to lower the ε' of the material. Besides excellent thermal stability with < 0.4% weight loss at 500 °C, adhesion testing on the material showed good particle-to-particle and particle-to-substrate adhesion. Moreover, the dielectric properties measured at 7.2 GHz using cavity perturbation method were equally impressive, with a ε' of 2.14 and $tan\ \delta$ of 0.001 at 5 wt% PI. This represents the first reported PTFE/PI core-shell nanoparticle, which also provides a high performance, solution processable dielectric material for AM.

6. Actively-tunable microwave substrates using P3HT/PCBM:PDMS composite blends

*The following section is anticipated to be submitted for publication in 2017.

6.1. Introduction

A variety of materials exist that exhibit advanced dielectric properties. Such materials can significantly enhance the dielectric properties of a substrate when present, thereby improving performance and extending the utility of devices. In particular, ferrites have been widely studied as magnetically tunable materials that display enhanced microwave properties, making possible actively tunable microwave devices.[65] Additionally, organic semiconductors can exhibit similar advanced dielectric properties and have been demonstrated as photo-tunable materials. In 2010, Su et al. designed an active frequency selective surface using P3HT.[66] Under illumination, the change in dielectric properties made possible a 12 GHz tunable filter. In 2015, Andy et al. demonstrated a 13.5% tunablility of a P3HT thin film at optical frequencies (220-325 GHz).[67] Additionally, in 2015 Hu et al. demonstrated an optically tunable Seebeck coefficient based on organic excited-state intramolecular proton-transfer (ESIPT) molecules in vertical thin-film thermoelectrics.[68] However, despite these successes, to date there are no known reports of an optically tunable dielectric substrate for microwave devices.

Organic polymers are widely considered an attractive alternative due to their functionality, relative low-cost, and favorable processing charactertistics.[69] P3HT is a polymerized thiophene, that when oxidized, can become conductive. Regioregular P3HT, a highly crystalline polymer, is considered the benchmark for semiconducting polymers due to it being readily and widely available, solution processable, and having attractive electrical properties. It has a highly planar backbone that is both electron rich and π-conjugated with a HOMO energy level of -4.6 eV. More importantly, P3HT

has a bandgap of 1.9 eV, suitable for photo-excitation of free carriers. When regioregularity exceeds 96%, charge carrier mobility can reach 0.1 $cm^2/V \cdot s$.[70] Coupled with its optical absorption properties, the high charge carrier mobility of P3HT makes it an ideal material for optical modulation of its properties, both by itself and as a component in composite blends. Furthermore, when blended with a n-type material such as [6,6]-Phenyl C61 butyric acid methyl ester (PCBM), one can distort the P3HT and induce dissociation of free electrons.[71] This blending of different band gaps creates a heterojunction that generates a greater number of free carriers than that of pure P3HT. It is expected that a polymer composite comprised of P3HT/PCBM supported in a PDMS matrix, will exhibit tunable microwave properties when optically illuminated.

This chapter presents a study of photo-tunable dielectric polymer composites at microwave frequencies of 1-6 GHz. Comprised of a blend of P3HT/PCBM together with a low-k polymer dielectric PDMS, the polymer composites result in a new class of microwave substrates with wide tunability of the relative permittivity. Hence, this material offers a new approach for the fabrication of advanced, high-performance microwave devices. Performance characteristics, namely impedance matching, together with the amenable manufacturing aspects make this material well suited for the engineering, fabrication, and utilization of microwave substrates.

6.2. Experimental

Materials

P3HT (RMI-001E) was purchased from Rieke Metals (Lincoln, NE) and used as received. P3HT was characterized for the regioregularity and molecule weights (see SI). PCBM (684430), PDMS

(761036), and chloroform (CX1056) were purchased from Sigma-Aldrich (St. Louis, MO) and used as received.

Preparation of P3HT/PCBM:PDMS-based multilayer microstrip

The polymer composite is made of P3HT/PCBM blend and PDMS. The ratio between P3HT and PCBM is 95 : 5. The ratio between the blend and PDMS is 1 : 1. The reason for using much more P3HT than PCBM in the blend is that the number of bulk heterojunctions (BHJ) formed in the composite can be significantly reduced so that a gradual increase of exciton generation rate and the balance of the rate between the charge carrier generation and recombination can be observed during the measurements. The reason for using PDMS to dilute the blend is that the mechanical strength of the polymer composite can be enhanced in compliance with the measurements. To prepare the polymer composite, the P3HT/PCBM blend was prepared by combining 50.0 mg of P3HT and 2.6 mg of PCBM along with 2.0 ml of chloroform and stirring at 300 rpm and 30 ˚C for 4 h, followed by the addition of 52.6 mg of PDMS and. The polymer composite solution was mixed thoroughly and was molded onto a copper ground plane using a two-piece silicone mold, rending a sample with suitable dimensional tolerances as required for microwave substrates. The filled molds were cured at 80 ˚C for 24 h under vacuum (25 mm Hg). A copper transmission line was later deposited onto the surface, as depicted in Figure 29.

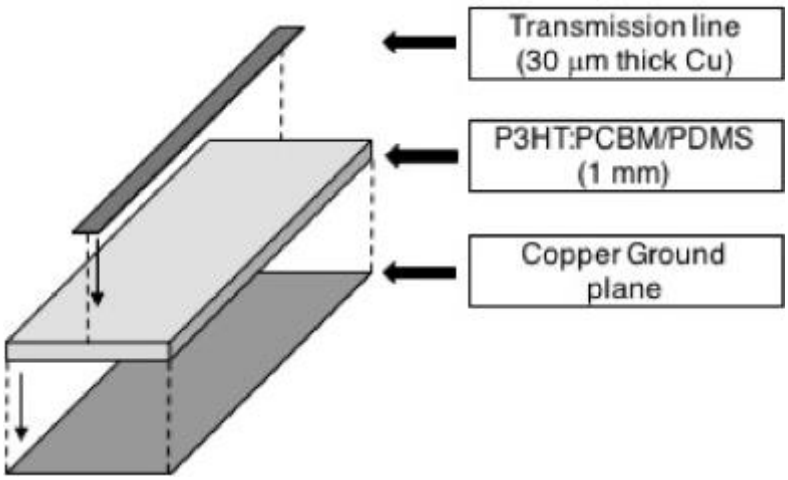

Figure 29. Graphical depiction of the multilayer microstrip based on P3HT:PCBM/PDMS.

Extraction of Dielectric Properties

To study the dielectric properties including relative permittivity (ε_r) and loss tangent ($tan\ \delta$) of the polymer composite, an experimental setup as shown in Figure 30 was designed. The microstrip was held by two test fixtures, which have edge-mount connectors attaching to the end of the copper transmission line. Subminiature "A" (SMA) connectors and cables were used and affixed to the connectors . The LED arrays (white light, spectrum centered at 532 nm) were placed on the top of the microstrip and the incident illumination was perpendicular to the microstrip surface. The illumination power density from the LED arrays was measured by a light meter (Omega HHLM3) and controlled with a rheostat to levels ranging from 0-80 mW/cm^2 during the measurements.

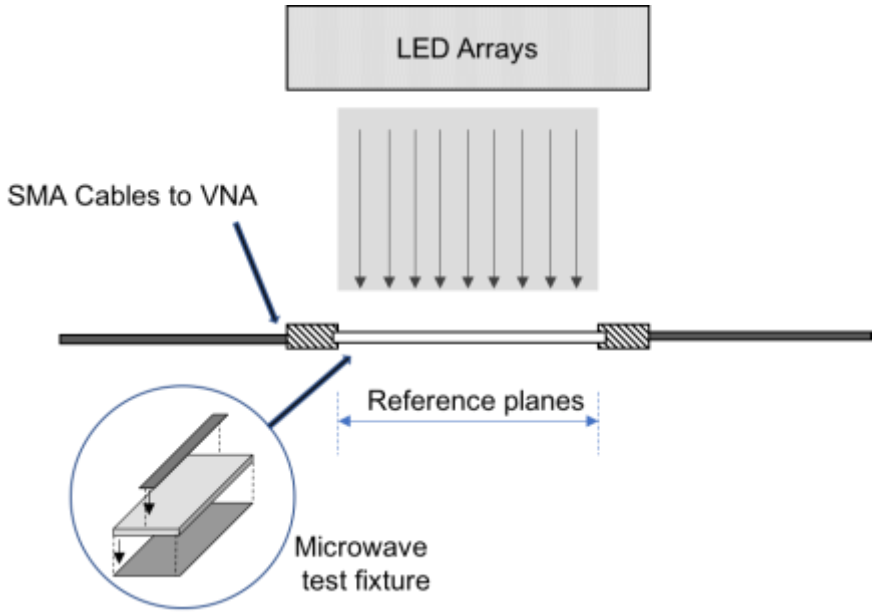

Figure 30. Schematic representation of the two-port microwave test fixture with the white LED light source.

To obtain the dielectric properties (relative permittivity, ε_r and loss tangent, $tan\ \delta$), S-parameter (S_{11}, S_{12}, S_{21}, S_{22}) measurements covering a range of 1-6 GHz were performed using the thru-reflect-line (TRL) method. A Hewlett-Packard HP8510C microwave test set was used to measure S-parameters. The reference planes were set at the edge of the microstrip fixture and seen in Figure 30. The measured S-parameters were used to extract the microwave properties of the polymer composite. A non-iterative, modified Nicholson-Ross-Weir formulation method was used to determine analytical values for the filling factors.[72]

The non-iterative method uses the following equations:

$$S_{11} = \frac{\Gamma(1 - T^2)}{(1 - \Gamma^2 T^2)} \tag{22}$$

$$S_{21} = \frac{T(1-\Gamma^2)}{(1-\Gamma^2 T^2)} \tag{23}$$

The S-parameters are the data output of the Vector Network Analyzer (VNA).

The reflection coefficient can be calculated:

$$\Gamma = X \pm \sqrt{X^2 - 1} \tag{24}$$

In terms of S-parameter, it is defined as

$$X = \frac{S_{11}^2 - S_{21}^2 + 1}{2S_{11}} \tag{25}$$

The transmission coefficient can be calculated:

$$T = \frac{S_{11}^2 + S_{21}^2 - \Gamma}{1 - (S_{11} + S_{21})\Gamma} \tag{26}$$

$$\frac{1}{\Lambda^2} = \left[\frac{\varepsilon_r \mu_r}{\lambda_0^2} - \frac{1}{\lambda_c^2}\right] = -\left[\frac{1}{2\pi L} ln\left[\frac{1}{T}\right]\right]^2 \quad (27)$$

where λ_0 is the free space wavelength and λ_c is the cutoff wavelength with:

$$\lambda_{og} = \frac{1}{\sqrt{\frac{1}{\lambda_0^2} - \frac{1}{\lambda_c^2}}} \quad (28)$$

which represents the wavelength in an empty cell.

The effective electromagnetic parameters are defined as:

$$\mu_{eff} = \frac{\lambda_{og}}{\Lambda}\left[\frac{1+\Gamma}{1-\Gamma}\right] \quad (29)$$

and

$$\varepsilon_{eff} = \frac{\lambda_{og}}{\Lambda}\left[\frac{1-\Gamma}{1+\Gamma}\right] \quad (30)$$

Using Γ and equation *X*, the effective parameters can be determined.

Therefore:

$$\mu_r = \mu_{eff} = \frac{1}{\Lambda}\left[\frac{1+\Gamma}{1-\Gamma}\right]\frac{1}{\sqrt{\frac{1}{\lambda_0^2}-\frac{1}{\lambda_c^2}}} \tag{31}$$

and

$$\varepsilon_r = \left[1-\frac{\lambda_0^2}{\lambda_c^2}\right]\varepsilon_{eff} + \frac{\lambda_0^2}{\lambda_c^2}\frac{1}{\mu_{eff}} \tag{32}$$

If used for non-magnetic material where $\mu_r = \mu_{eff} = 1$, then the effective complex permittivity is:

$$\varepsilon_{eff} = \varepsilon_{eff}(\mu_{eff})^n = \left[\frac{1-\Gamma}{1+\Gamma}\right]^{n-1}\left[\frac{\lambda_{og}}{\Lambda}\right]^{n+1} \tag{33}$$

where $n=1$

$Tan\ \delta$ can be calculated by first converting S-parameters into ABCD parameters then calculating the complex propagation constant $\gamma = \alpha + j\beta$ where α is attenuation constant and β is phase constant. Real and imaginary parts of the complex permittivity of a substrate can be calculated using the known approximations:[13]

$$\varepsilon_r^{'} = \frac{c^2}{\omega^2}(\beta^2) \tag{34}$$

and

$$\varepsilon_r^{''} = \frac{c^2}{\omega^2}(2\alpha_d\beta) \tag{35}$$

Tan δ of the material is then:

$$tan\,\delta = \frac{\varepsilon_r^{''}}{\varepsilon_r^{'}} \tag{36}$$

The exciton binding energy can be calculated:

$$E_b = \frac{q^2}{4\pi\varepsilon_r^{'}\,\varepsilon_0 R} \tag{37}$$

6.3. Results and discussion

Figure 31 shows the extracted ε_r' of the polymer composite with the increase of the illumination level (P, 0-80 mW/cm^2) at different microwave frequencies (f, 1-6 GHz). It is noted that the change of the ε_r' exhibited three phases with the increase of the illumination level while a higher ε_r' was obtained with a higher frequency. This can be understood by the exciton generation and dissociation and the charge generation and recombination of the P3HT/PCBM in the polymer composite by calculating the exciton binding energy (E_b) from ε_r', as depicted in Figure 32. At low illumination level (P < 30 mW·cm^{-2}, region 1), ε_r' shows an approximate linear increase with P,

corresponding to an approximate linear relationship between E_b and P, which indicates an increase in exciton generation rate. However, the generated excitons do not readily dissociate into free charge carriers due to a high E_b in the range of 0.30-0.36 eV. Further increase of the illumination level (30 mW/cm^2 < P < 40 mW/cm^2, region 2) decreases the E_b to less than 0.30 eV, which promotes the dissociation of exciton and the generation of free charge carriers. Therefore, a rapid increase of ε_r' is observed in this region. At high illumination level (P > 40 mW/cm^2, region 3), ε_r' reaches a plateau, suggesting the balance between charge generation and recombination, corresponding to a constant E_b. In addition, a good linear relationship was observed between f and ε_r', as shown in Figure 33, suggesting that ε_r' can be finely tuned by f. Calculated from the minimum and maximum values from the measurements, the overall tunability of ε_r' depending on f and P are 8% and 21%, respectively.

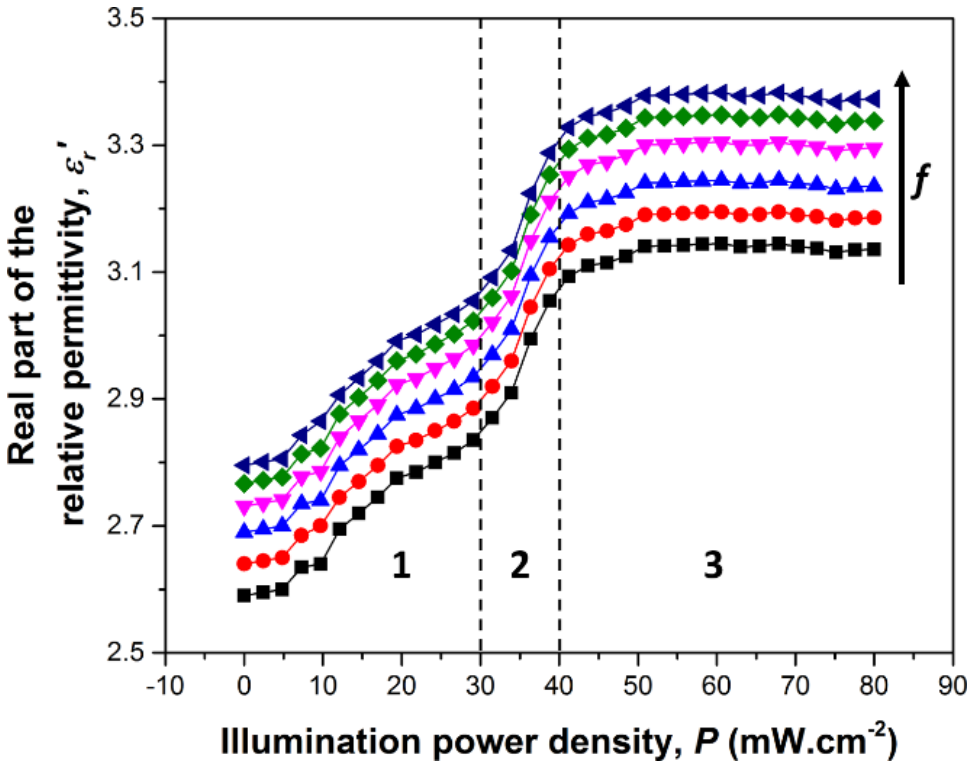

Figure 31. Extracted ε_r' of the polymer composite with the increase of P at different f.

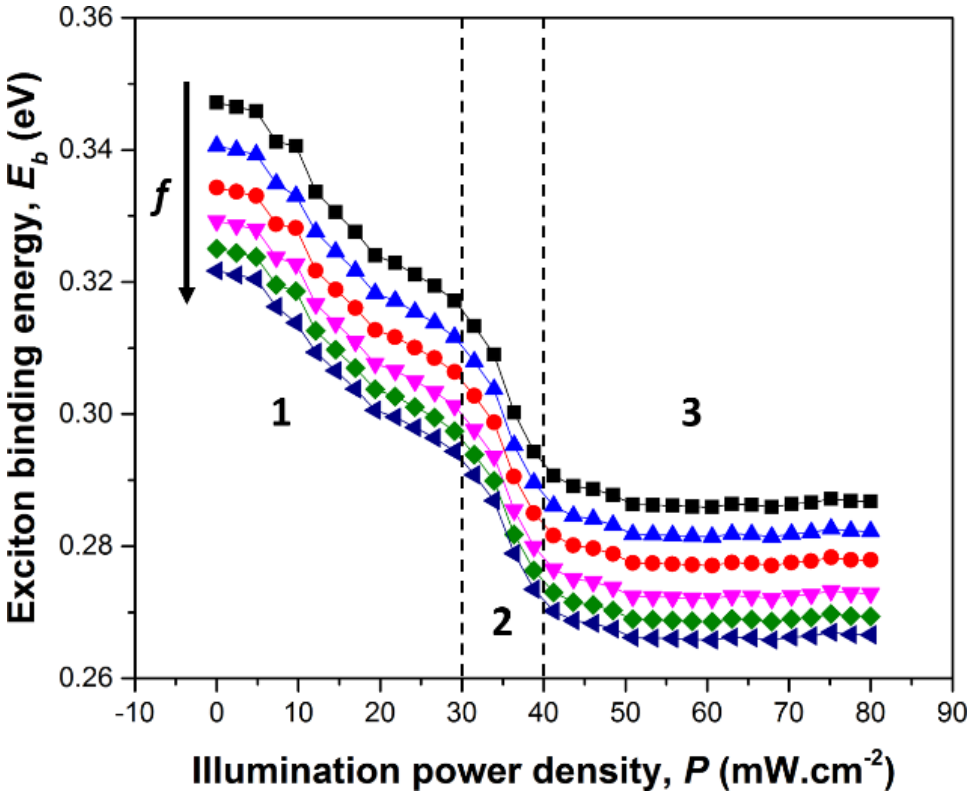

Figure 32 Calculated E_b of the polymer composite with the increase of P at different f

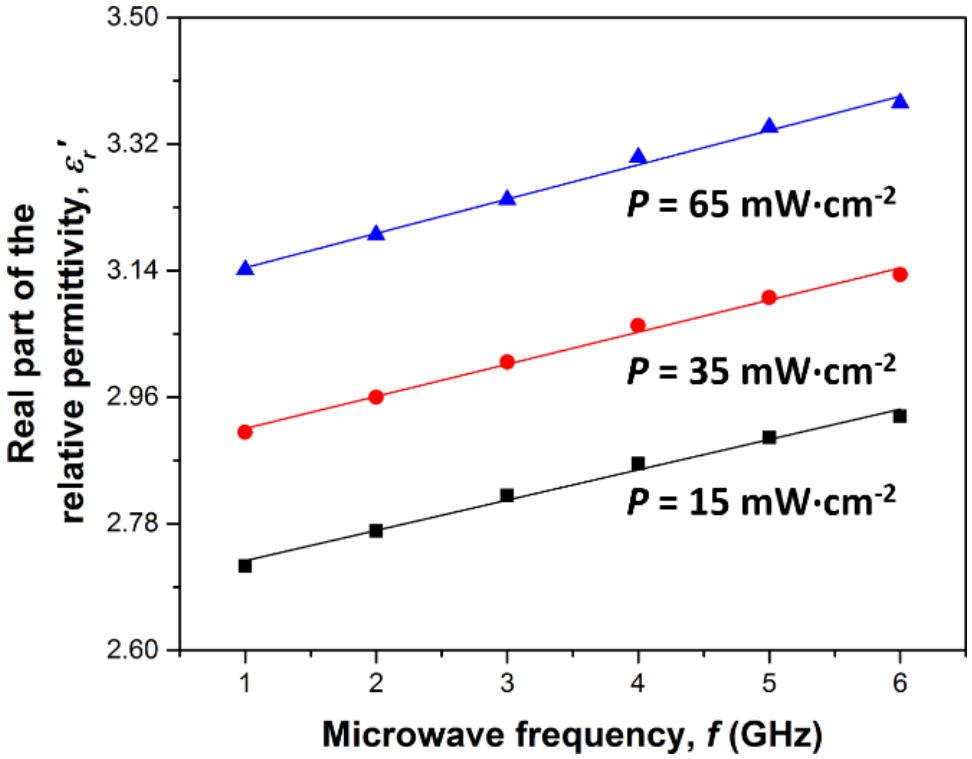

Figure 33 Linear relationship between ε_r' and *f* under different *P*.

Besides ε_r', *tan δ* representing the dielectric loss, is another important dielectric parameter. Figure 34 depicts the extracted *tan δ* of the polymer composite with the increase of *P* at different *f*. It is noted that tan δ increases and then decreases with the increases of *P* while no obvious dependence was observed with *f*. The maximum region of *tan δ* is between 35 mW/cm^2 and 45 mW/cm^2, which matches the region of the rapid decrease of E_b. This observation is reasonable because a high rate of exciton dissociation/charge carrier generation significantly disrupts the energetic state of the system and thus its dielectric properties are affected. Small *tan δ* values were only observed when the rate of charge carrier generation is minimal (low *P*) or the charge carrier generation and recombination reaches the equilibrium (high *P*).

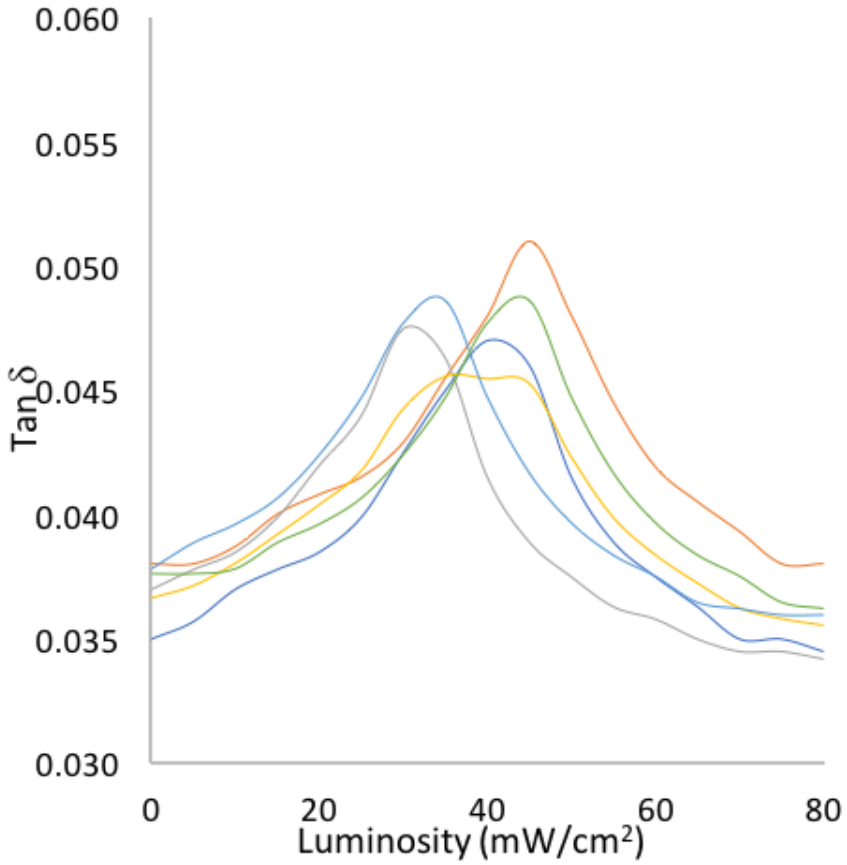

Figure 34. Extracted tan δ for P3HT/PCBM:PDMS 50 wt% polymer composite.

To evaluate the accuracy of the mathematical extraction of properties, the attenuation can be calculated using the extracted properties and then compared to the attenuation derived from the S-parameters taken from the VNA. The calculated attenuation (α) from the extracted properties is given as:[73]

$$\alpha = \frac{\pi\sqrt{2\delta_r'}}{\left[{}^{c}/_{2\pi f}\right]}\left(\sqrt{1+tan^2\delta}-1\right)^{1/2} \quad (38)$$

The measured attenuation is calculated from S-parameters as:[74]

$$e^{-(\alpha+j\beta)L} = \left(\frac{1 - S_{11}^2 + S_{21}^2}{2S_{21}} \pm K\right)^{-1} \tag{39}$$

where

$$K = \left[\frac{(S_{11}^2 - S_{21}^2 + 1)^2 - (2S_{11})^2}{(2S_{21})^2}\right]^{1/2} \tag{40}$$

Figure 35. Compares the attenuation at 6 GHz derived from the extracted properties with the attenuation calculated directly from S-parameters. Good agreement is evident, which verifies the accuracy of the extraction methodology.

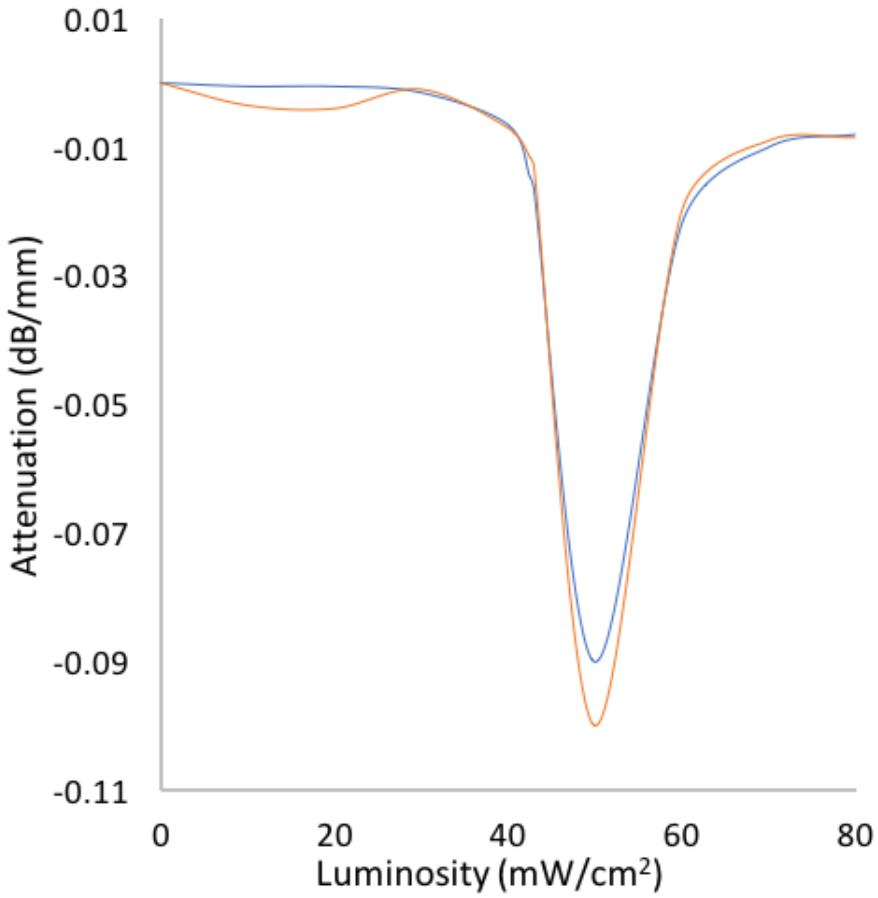

Figure 35. Attenuation derived from S-parameters compared with attenuation calculated using extracted material properties.

6.4. Conclusions

Advanced microwave properties of a polymer composite comprised of P3HT/PCBM blended with 50 wt% PDMS have been extracted in the microwave frequencies of 1-6 GHz. The material properties extraction method is based on a non-iterative mathematical method using TRL calibration. Tunabilty of the permittivity as high as 20% was demonstrated and an increase of 34% of the loss tangent, all under 70 mW/cm^2 illumination. These properties make this material very useful for the design of actively tunable devices such as antennas, phase shifters, and switches. In

addition, this material in its initial state can be made amenable for non-contact deposition techniques such as drop casting, aerosol spraying, or even ink jetting, making possible a microwave device that is 100% additively manufactured.

7. Closing remarks and conclusions

7.1. General conclusions

This work has explored the dielectric phenomena of novel polymeric materials with an aim of eventually deploying them in AM processes. We first examined a facile method of core-shell particle synthesis that enabled the room temperature aerosol deposition of a PTFE/PA core-shell nanoparticle. A PA shell made possible a dense, very homogenous composite of PTFE nanoparticles within the PA matrix. The was due to an annealing step that modestly melts the PA shell. While the dielectric properties were suitable for AM use, the thermos-physical properties of the PA shell were not suitable, namely the low T_g. In addition, PA's affinity for water is undesirable. However, this initial foray into core-shell synthesis proved that a viable strategy exists to enable the deposition of PTFE in a controlled manner with homogenous results. From here, a brief study of various polyimides elucidated the relationship between these polymer structures and the resulting properties, namely dielectric properties. Indeed, a strong correlation exists between polymer rigidity and dielectric constant, due to the chain packing efficiency promoted via stiff, rigid polymer backbones. Furthermore, this study clearly showed a markedly lower dielectric constant due to the effect of the low polarizability of fluorine, known to be the most electronegative element in nature and therefore correspondingly low polarizability. The next phase of this work involved taking the prior knowledge of PI's and combining that with the initial core-shell synthesis of the PTFE/PA nanoparticles. The result was the first ever report of a PTFE/PI core-shell nanoparticle with outstanding dielectric properties in strong agreement with theoretical predictions. The excellent high temperature stability of the PI's were an ideal candidate to replace the PA, not to mention the ideal dielectric properties. The resulting PTFE/PI core-shell

nanoparticle shows strong promise as an advanced material for AM processes, particularly for microwave device fabrication. And finally, and most significant scientific contribution was the formulation of a semiconducting polymer blend of P3HT/PCBM coupled with PDMS to form a mechanically robust substrate capable of actively tuning the dielectric properties via ordinary white light illumination. Under maximum illumination, a tunabilty of 20% was realized, indicating that yet another advanced material capable of AM processes. However, in this case, the applications are numerous and technologically significant including advanced microwave devices such as phase shifters, variable integrated capacitors, and filters.

In conclusion, this work has demonstrated two advanced polymeric materials suitable for the AM of microwave devices. No doubt there remains significant work to field these materials, but a solid foundation has been laid for which subsequent studies can be tailored.

7.2. Closing Remarks

One topic I have not covered is the experience of a non-traditional student and the personal growth therein. I began this journey as a mid-level industry veteran, in most cases 15 years senior to most of my fellow UW students. I could write at length about all the times I knew a better way or a safer method but little would be learned from that discussion. What I found most valuable during the course of my tenure at UW was that the path to success is paved with failure. I changed advisors three times, most recently after two years of making little progress towards a PhD. Yet, I managed to gain a determined focus and with the help of many people, found myself on schedule making continual progress. And much like my research, the results have lead to a renewed confidence that I can bring with me upon my return to industry.

List of Publications

O'Keefe, S. and Luscombe, C. K., Microwave dielectric properties of polytetrafluoroethylene-polyacrylate composite films made via aerosol deposition. Polymer International **2016,** *65* (7), 820-826.

O'Keefe, S., Li, Y. and Luscombe, C. K., Solution processed low-k dielectric core-shell nanoparticles for additive manufacturing of microwave devices. Journal of Applied Polymer Science., (accepted)

O'Keefe, S., Li, Y. and Luscombe, C. K., P3HT/PCBM:PDMS photo-tunable composites for microwave devices, (pending review).

8. References

1. Gibson, I.; Rosen, D. W.; Stucker, B., *Additive Manufacturing Technologies: Rapid Prototyping to Direct Digital Manufacturing*. Springer US: Boston, MA: Boston, MA, 2010.

2. Melchels, F. P. W.; Domingos, M. A. N.; Klein, T. J.; Malda, J.; Bartolo, P. J.; Hutmacher, D. W., Additive manufacturing of tissues and organs. *Progress in Polymer Science* **2012,** *37* (8), 1079-1104.

3. Brown, G. B., Validity of the Clausius-Mosotti formula. *Nature* **1942,** *150*, 661-662.

4. Adler, S. L., QUANTUM THEORY OF DIELECTRIC CONSTANT IN REAL SOLIDS. *Physical Review* **1962,** *126* (2), 413-+.

5. Basics of Measuring the Dielectric Properties of Materials. http://cp.literature.agilent.com/litweb/pdf/5989-2589EN.pdf.

6. Hougham, G. G.; Jean, Y. C., Relative Contributions of Polarizability and Free Volume in Reduction of Refractive Index and Dielectric Constant with Fluorine Substitution in Polyimides by Positron Annihilation Spectroscopy. *Macromolecular Chemistry and Physics* **2014,** *215* (1), 103-110.

7. Free Volume. www.doitpoms.ac.uk/tlplib/glass-transition/free-volume.php.

8. Hougham, G.; Tesoro, G.; Viehbeck, A., Influence of free volume change on the relative permittivity and refractive index in fluoropolyimides. *Macromolecules* **1996,** *29* (10), 3453-3456.

9. Kronig, R. D. L., On the theory of dispersion of x-rays. *Journal of the Optical Society of America and Review of Scientific Instruments* **1926,** *12* (6), 547-557.

10. Cole, K. S.; Cole, R. H., Dispersion and absorption in dielectrics I. Alternating current characteristics. *Journal of Chemical Physics* **1941,** *9* (4), 341-351.

11. O'Keefe, S.; Luscombe, C. K., Microwave dielectric properties of polytetrafluoroethylene-polyacrylate composite films made via aerosol deposition. *Polymer International* **2016,** *65* (7), 820-826.

12. Wangsness, R. K., *Electromagnetic fields*. 2nd ed. ed.; New York : Wiley: New York, 1986.

13. Pozar, D. M., *Microwave Engineering*. 4th ed. ed.; Hoboken : Wiley: Hoboken, 2012.

14. Subodh, G.; Joseph, M.; Mohanan, P.; Sebastian, M. T., Low dielectric loss polytetrafluoroethylene/TeO2 polymer ceramic composites. *Journal of the American Ceramic Society* **2007,** *90* (11), 3507-3511.

15. Banks, R. E.; Smart, B. E.; Tatlow, J. C., *Organofluorine Chemistry: Principles and Commercial Applications*. Plenum Press: New York, 1994.

16. Davidson, T.; Gounder, R. N.; Weber, D. K.; Wecker, S. M., *A Perspective on Solid State Microstructure in Polytetrafluoroethylene, in Fluoropolymers 2: Properties*. Plenum Press: New York, 1999.

17. Giani, E.; Sparnacci, K.; Laus, M.; Palamone, G.; Kapeliouchko, V.; Arcella, V., PTFE-polystyrene core-shell nanospheres and nanocomposites. *Macromolecules* **2003,** *36* (12), 4360-4367.

18. Hambir, S. S.; Jog, J. P.; Nadkarni, V. M., STRENGTH DEVELOPMENT IN POWDER PROCESSING OF POLY(TETRAFLUOROETHYLENE). *Polymer Engineering and Science* **1994,** *34* (13), 1065-1069.

19. Nuttall, K. I.; Buiu, O.; Obreja, V. V. N., Surface leakage current related failure of power silicon devices operated at high junction temperature. *Microelectronics Reliability* **2003,** *43* (9-11), 1913-1918.

20. Sparnacci, K.; Antonioli, D.; Deregibus, S.; Laus, M.; Poggio, T.; Kapeliouchko, V.; Palamone, G.; Zuccheri, G.; Passeri, R., PTFE-Based Core-Soft Shell Nanospheres and Soft Matrix Nanocomposites. *Macromolecules* **2009,** *42* (10), 3518-3524.

21. Sheen, J., Study of microwave dielectric properties measurements by various resonance techniques. *Measurement* **2005,** *37* (2), 123-130.

22. Cui, X.; Zhong, S.; Zhang, H.; Gu, Q.; Li, J.; Wang, H., Preparation and characterization of polytetrafluoroethylene-polyacrylate core-shell nanoparticles. *Polymers for Advanced Technologies* **2007,** *18* (7), 544-548.

23. Laihonen, S. J.; Gustafsson, A.; Gafvert, U.; Schutte, T.; Gedde, U. W., Area dependence of breakdown strength of polymer films: Automatic measurement method. *IEEE Trans. Dielectr. Electr. Insul.* **2007,** *14* (2), 263-274.

24. Zakri, T.; Laurent, J. P.; Vauclin, M., Theoretical evidence for 'Lichtenecker's mixture formulae' based on the effective medium theory. *J Phys D-Appl Phys* **1998,** *31* (13), 1589-1594.

25. Ruppin, R., Validity range of Maxwell-Garnet Theory. *Phys Status Solidi B* **1978,** *87* (2), 619-624.

26. Kirkpatr, S., Classical transport in disordered media - scaling and effective-medium theories. *Physical Review Letters* **1971,** *27* (25), 1722-1739.

27. O'Keefe, S.; Li, Y.; Luscombe, C. K., Solution processed low-k dielectric core-shell nanoparticles for the additive manufacturing of microwave devices. *Journal of Applied Polymer Science* **2017,** *134* (41).

28. Liaw, D. J.; Wang, K. L.; Huang, Y. C.; Lee, K. R.; Lai, J. Y.; Ha, C. S., Advanced polyimide materials: Syntheses, physical properties and applications. *Progress in Polymer Science* **2012,** *37* (7), 907-974.

29. Ghosh, M. K.; Mittal, K. L., *Polyimides : fundamentals and applications*. New York : Marcel Dekker: New York, 1996.

30. Mittal, K. L., *Polyimides and other high temperature polymers. Volume 2 Synthesis, characterization and applications*. Leiden : Brill: Leiden, 2003.

31. Fryd, M., Structure — Tg Relationship in Polyimides. In *Polyimides: Synthesis, Characterization, and Applications. Volume 1*, Mittal, K. L., Ed. Springer US: Boston, MA, 1984; pp 377-383.

32. H Ohya, V. K., SI Semenova, *Polyimide Membranes: Applications, fabrications, and properties*. Kodansha Ltd: Tokyo, 1996.

33. Sroog, C. E., Polyimides. *Journal of Polymer Science: Macromolecular Reviews* **1976,** *11* (1), 161-208.

34. Kazama, S.; Teramoto, T.; Haraya, K., Carbon dioxide and nitrogen transport properties of bis(phenyl)fluorene-based cardo polymer membranes. *Journal of Membrane Science* **2002,** *207* (1), 91-104.

35. Wozniak, A. I.; Yegorov, A. S.; Ivanov, V. S.; Igumnov, S. M.; Tcarkova, K. V., Recent progress in synthesis of fluorine containing monomers for polyimides. *Journal of Fluorine Chemistry* **2015,** *180*, 45-54.

36. Berman, B., 3-D printing: The new industrial revolution. *Business Horizons* **2012,** *55* (2), 155-162.

37. Kietzmann, J.; Pitt, L.; Berthon, P., Disruptions, decisions, and destinations: Enter the age of 3-D printing and additive manufacturing. *Business Horizons* **2015,** *58* (2), 209-215.

38. Hock, L., 3-D Printing: A New Manufacturing Staple. *R&D Magazine* **2014,** *56* (2), 18-19.

39. Carlson, A.; Bowen, A. M.; Huang, Y. G.; Nuzzo, R. G.; Rogers, J. A., Transfer Printing Techniques for Materials Assembly and Micro/Nanodevice Fabrication. *Advanced Materials* **2012,** *24* (39), 5284-5318.

40. Lewis, G. K.; Schlienger, E., Practical considerations and capabilities for laser assisted direct metal deposition. *Materials & Design* **2000,** *21* (4), 417-423.

41. Gu, D. D.; Meiners, W.; Wissenbach, K.; Poprawe, R., Laser additive manufacturing of metallic components: materials, processes and mechanisms. *International Materials Reviews* **2012,** *57* (3), 133-164.

42. Levy, G. N.; Schindel, R.; Kruth, J. P., Rapid manufacturing and rapid tooling with layer manufacturing (LM) technologies, state of the art and future perspectives. *Cirp Annals-Manufacturing Technology* **2003,** *52* (2), 589-609.

43. Ochoa, I.; Hatzikiriakos, S. G., Paste extrusion of polytetrafluoroethylene (PTFE): Surface tension and viscosity effects. *Powder Technology* **2005,** *153* (2), 108-118.

44. Scheirs, J., *Polymer recycling : science, technology, and applications*. Chichester

New York : Wiley: Chichester

New York, 1998.

45. Xiang, F.; Wang, H.; Yao, X., Preparation and dielectric properties of bismuth-based dielectric/PTFE microwave composites. *Journal of the European Ceramic Society* **2006,** *26* (10-11), 1999-2002.

46. Thomas, S.; Deepu, V. N.; Mohanan, P.; Sebastian, M. T., Effect of filler content on the dielectric properties of PTFE/ZnAl2O4-TiO2 composites. *Journal of the American Ceramic Society* **2008,** *91* (6), 1971-1975.

47. Thomas, S.; Raman, S.; Mohanan, P.; Sebastian, M. T., Effect of coupling agent on the thermal and dielectric properties of PTFE/Sm2Si2O7 composites. *Composites Part a-Applied Science and Manufacturing* **2010,** *41* (9), 1148-1155.

48. Jin, S. Q.; Qiu, X.; Huang, B. Y.; Wang, L. X.; Zhang, Q. T.; Fu, Z. X., Dielectric properties of modified BNT/PTFE composites for microwave RF antenna applications. *Journal of Materials Science-Materials in Electronics* **2016,** *27* (8), 8378-8383.

49. Jin, S. Q.; Wang, L. X.; Wang, Z. F.; Huang, B. Y.; Zhang, Q. T.; Fu, Z. X., Dielectric properties of modified SrTiO3/PTFE composites for microwave RF antenna applications. *Journal of Materials Science-Materials in Electronics* **2015,** *26* (10), 7431-7437.

50. Antonioli, D.; Deregibus, S.; Panzarasa, G.; Sparnacci, K.; Laus, M.; Berti, L.; Frezza, L.; Gambini, M.; Boarino, L.; Enrico, E.; Comoretto, D., PTFE-PMMA core-shell colloidal particles as building blocks for self-assembled opals: synthesis, properties and optical response. *Polymer International* **2012,** *61* (8), 1294-1301.

51. Kapeliouchko, V.; Palamone, G.; Poggio, T.; Zuccheri, G.; Passeri, R.; Sparnacci, K.; Antonioli, D.; Deregibus, S.; Laus, M., PMMA-Based Core-Shell Nanoparticles with Various PTFE Cores. *Journal of Polymer Science Part a-Polymer Chemistry* **2009,** *47* (11), 2928-2937.

52. Misra, A. C.; Tesoro, G.; Hougham, G.; Pendharkar, S. M., Synthesis and Properties of Some New Fluorine-Containing Polyimides. *Polymer* **1992,** *33* (5), 1078-1082.

53. Minges, M. L.; Committee, A. S. M. I. H., *Electronic materials handbook*. Materials Park, OH : ASM International: Materials Park, OH, 1989.

54. Facinelli, J. V.; Gardner, S. L.; Dong, L.; Sensenich, C. L.; Davis, R. M.; Riffle, J. S., Controlled molecular weight polyimides from poly(amic acid) salt precursors. *Macromolecules* **1996,** *29* (23), 7342-7350.

55. Birnbaum, G.; Franeau, J., Measurement of the Dielectric Constant and Loss of Solids and Liquids by a Cavity Perturbation Method. *Journal of Applied Physics* **1949,** *20* (8), 817-818.

56. Sheen, J., Measurements of microwave dielectric properties by an amended cavity perturbation technique. *Measurement* **2009,** *42* (1), 57-61.

57. Zhou, H. R.; Yu, W. M.; Qu, C. Y.; Liu, C. W.; Wang, D. Z., Facile one-step synthesis of PI/Fe3O4 composite microspheres from poly(amic acid) triethylamine salts and Fe(III) ion. *Journal of Materials Science - Materials in Electronics* **2015,** *26* (12), 9789-9794.

58. Ramani, R.; Das, V.; Singh, A.; Ramachandran, R.; Amarendra, G.; Alam, S., Free Volume Study on the Origin of Dielectric Constant in a Fluorine-Containing Polyimide Blend: Poly(vinylidene fluoride-co-hexafluoro propylene)/Poly(ether imide). *Journal of Physical Chemistry B* **2014,** *118* (42), 12282-12296.

59. Nakamura, N.; Matsunaga, N.; Higashi, K.; Shimada, M.; Miyajima, H.; Yamada, M.; Enomoto, Y.; Hasegawa, T.; Shibata, H. In *A Study of Water Absorption Induced-Dielectric Constant Increase and Its Suppression on Copper Damascene Interconnect Structure with Porous Low-k (k=2.3) Dielectrics*, 2006 International Interconnect Technology Conference, 5-7 June 2006; 2006; pp 119-121.

60. Suwa, T.; Takehisa, M.; Machi, S., MELTING AND CRYSTALLIZATION BEHAVIOR OF POLY(TETRAFLUOROETHYLENE) - NEW METHOD FOR MOLECULAR-WEIGHT MEASUREMENT OF POLY(TETRAFLUOROETHYLENE) USING A DIFFERENTIAL SCANNING CALORIMETER. *Journal of Applied Polymer Science* **1973,** *17* (11), 3253-3257.

61. Kurabayashi, K.; Asheghi, M.; Touzelbaev, M.; Goodson, K. E., Measurement of the thermal conductivity anisotropy in polyimide films. *Journal of Microelectromechanical Systems* **1999,** *8* (2), 180-191.

62. ASTM F2252/F2252M-13e1 Standard Practice for Evaluatig Ink or Coating Adhesion to Flexible Packaging Materials Using Tape. West Conshohocken, PA, 2013.

63. Ratta, V.; Stancik, E. J.; Ayambem, A.; Pavatareddy, H.; McGrath, J. E.; Wilkes, G. L., A melt-processable semicrystalline polyimide structural adhesive based on 1,3-bis(4-aminophenoxy)benzene and 3,3 ',4,4 '-biphenyltetracarboxylic dianhydride. *Polymer* **1999,** *40* (7), 1889-1902.

64. Poon, S. J.; Petersen, A. S., Effective medium approach to thermal conductivity: applying to core-shell nanocomposites. *Emerging Materials Research* **2012,** *1* (6), 286-291.

65. Pettiford, C.; Lou, J.; Russell, L.; Sun, N. X., Strong magnetoelectric coupling at microwave frequencies in metallic magnetic film/lead zirconate titanate multiferroic composites. *Applied Physics Letters* **2008,** *92* (12).

66. Su, H.; Liu, X.; Li, D.; Chen, X.; Parini, C. G.; Kreouzis, T., Design and Analysis of Active Frequency Selective Surfaces with Organic Semiconductor. In *21st International Symposium on Space Terahertz Technology*, Oxford, 2010.

67. Andy, A. S.; Sushko, O.; Kreouzis, T.; Donnan, R. S., Optically-Tunable Organic Semiconductor Heterojunction P3HT-PCBM for millimeter-wave applications. In *IEEE*, Hong Kong, 2015.

68. Hu, D.; Liu, Q.; Tisdale, J.; Nam, H.; Park, S. Y.; Wang, H.; Urbas, A.; Hu, B., Optically tunable Seebeck effect from intramolecular proton-transfer materials in organic vertical thin-film thermoelectric device. *Organic Electronics* **2015,** *26*, 117-120.

69. Mazzio, K. A.; Luscombe, C. K., The future of organic photovoltaics. *Chemical Society Reviews* **2015,** *44* (1), 78-90.

70. Jimison, L. H. Understanding Microstructure and Charge Transport in Semicrystalline Polythiophenes. Stanford University, 2011.

71. Irwin, M. D.; Buchholz, B.; Hains, A. W.; Chang, R. P. H.; Marks, T. J., p-Type semiconducting nickel oxide as an efficiency-enhancing anode interfacial layer in polymer bulk-heterojunction solar cells. *Proceedings of the National Academy of Sciences of the United States of America* **2008,** *105* (8), 2783-2787.

72. Boughriet, A. H.; Legrand, C.; Chaperon, A., Noniterative stable transmission/reflection method for low-loss material complex permittivity determination. *IEEE Transactions on Microwave Theory and Techniques* **1997,** *45* (1), 52-57.

73. Weir, W. B., Automatic measurement of complex dielectric constant and permeability at microwave frequencies. *IEEE* **1974,** *62* (1), 33-36.

74. Eisenstadt, W.; Eo, Y., S-parameter-based IC interconnect transmission line characterization. *IEEE Trans. Common. Hybrids, Manuf. Techno.* **1992,** *15* (4), 483-490.